RSC Sustainability

ROYAL SOCIETY OF CHEMISTRY

PAPER

View Article Online
View Journal

Cite this: DOI: 10.1039/d6su00024j

The use of whole Hawaiian macroalgae to engineer bioplastics and adhesives for wood-particleboards

Ian R. Campbell, †[a] Ty Shitanaka, †[b] Hannah M. Egan,[c] Manpreet Kaur,[b] Samir Kumar Khanal *[bd] and Eleftheria Roumeli *[a]

Production of novel materials from sustainable biological matter (biomatter) can contribute to the development of a global, circular bioeconomy. Among potential feedstocks, macroalgae stand out due to their fast growth rates and richly diverse biochemical composition. However, very few studies demonstrate the direct conversion of whole macroalgal biomatter into bulk materials and also perform comprehensive biochemical characterization. Here, we present a detailed, species-resolved compositional and macromolecular analysis of four native Hawaiian macroalgae, including carbohydrate speciation, protein molecular weight distributions, lipid profiles, and inorganic content. Each macroalgal species was then processed directly, without chemical pretreatment or fractionation, into two structurally distinct bioproduct classes: self-bonded bioplastics and algae-bonded wood particleboards. We characterized the mechanical properties and micromorphology of all bioproducts, as well as the flame resistance and seawater-biodegradation of selected materials, to establish structure–property relationships across species and material classes. The Hawaiian macroalgae exhibited carbohydrate, protein, lipid, and organic sulfate contents of 58–69 wt%, 5–12 wt%, 2–10 wt%, and 1–39 wt%, respectively, and species-specific sulfated polysaccharides were identified. Green macroalgae displayed broader protein molecular weight distributions (15–75 kDa) than red macroalgae (15–20 kDa). Bioplastics made from the red macroalgae exhibited higher flexural strength (46–70 MPa) and flexural modulus (8–9 GPa) compared to those from the green macroalgae (29–32 MPa, flexural strength; 5 GPa, flexural modulus). Differences in the bioplastic mechanical properties were correlated with differences in the macroalgal powder particle size distributions and protein characteristics. In wood particleboards bonded by macroalgal biomatter, the addition of 40% algae by weight improved the flexural strength and flexural modulus by 180–500% and 62.5–112.5%, respectively. All of the macroalgae-bonded wood particleboards also impressively self-extinguished in approximately 10 seconds, compared to the wood control which was completely consumed by flames. Overall, this work demonstrates that whole, minimally processed macroalgal biomatter can be directly transformed into multiple mechanically relevant material classes while retaining performance-relevant chemical complexity. Beyond the demonstrated bioplastics and particleboards, the comprehensive compositional dataset reported here provides a reference for the broader valorization of native macroalgal biomatter through diverse material and chemical pathways.

Received 14th January 2026
Accepted 3rd April 2026

DOI: 10.1039/d6su00024j

rsc.li/rscsus

1 Introduction

Macroalgae (seaweeds) have emerged as one of the most promising bioresources in the global search for renewable, environmentally benign raw materials. Between 2000 and 2018, global macroalgae aquaculture grew by 6.2% per year, largely because of its accessibility, high productivity, and inherent ecological benefits.[1] Macroalgae cultivation can occur in land-based tanks, in nearshore or offshore waters, and in integrated multi-trophic aquaculture systems.[2] Unlike terrestrial feedstocks such as corn or lignocellulosic biomass, macroalgae cultivation does not require arable land nor specialized equipment.[3] Furthermore, as macroalgae grow, they regulate the local concentrations of nutrients and pollutants, provide habitat for fish and invertebrates, and reduce the effects of ocean acidification.[4] Finally, many species grow rapidly; for example, some strains of *Ulva*, one of the most ubiquitous and widely distributed macroalgae, grow up to 15–22% fresh weight per day under

[a]*School of Materials Science and Engineering, The University of Washington, WA 98105, USA. E-mail: eroumeli@uw.edu*

[b]*Department of Molecular Biosciences and Bioengineering, University of Hawai'i at Mānoa, Honolulu, HI 96822, USA. E-mail: khanal@hawaii.edu*

[c]*GlycoMIP, Fralin Life Sciences Institute, Virginia Polytechnic Institute and State University, Blacksburg, VA 24061, USA*

[d]*Department of Civil and Environmental Engineering, The Hong Kong University of Science and Technology, Clear Water Bay, Kowloon 999077, Hong Kong. E-mail: cekhanal@ust.hk*

† These authors contributed equally to this work.

optimal conditions.[5] Rapid growth rates not only enable scalable manufacturing of algal bioproducts, but also indicate potential for contributions to carbon capture.[6,7] Taken together, these attributes position macroalgae cultivation as an attractive avenue for sustainable economic development, particularly for coastal regions of tropical and developing countries.

Although promising, there are several challenges with the large-scale cultivation of macroalgae. Current aquaculture operations occupy only 0.04% of the area of wild macroalgae habitat.[1] While this indicates that there is significant scope for the acceleration of macroalgae cultivation, due consideration should be afforded to responsible expansion and environmental preservation. Because of their adaptability and rapid growth, if not carefully controlled, macroalgae can escape into the surrounding environment, establish themselves, and become invasive species, as exemplified by the spread of *Kappaphycus* sp., *Eucheuma* sp., and *Gracilaria salicornia* in Hawai'i.[8] These alien red macroalgae exhibit combinations of functional traits (salinity tolerance, wave tolerance, substrate adaptability, and non-palatability) that are scarcely seen in native species, and have allowed their proliferation, causing loss of biodiverse habitats, functional diversity, and ecosystem services. Concerningly, another red alga, *Chrondria tumulosa*, has been traveling rapidly down the Hawaiian Island chain and could entrench itself alongside these established invasive algae.[8] To avoid further issues related to unregulated establishment and proliferation of invasive macroalgae, aquaculture operations could instead utilize highly productive local species. By cultivating locally available macroalgae, farmers can limit engineering controls required to restrict the spread of alien species, while also increasing efficiency and lowering cost.

The biological and compositional diversity of macroalgae further qualifies them as propitious bioresources. Macroalgae are broadly categorized into three different phyla, mainly based on their phenotype: green algae (Chlorophyta), red algae (Rhodophyta), and brown algae (Phaeophyta). Algae of the three phyla vary significantly from one another; individual species are classified not only by their pigment, but also by their morphology and composition. Each of the three phyla contains unique polysaccharides, proteins, and lipids that often cannot be found in terrestrial bioresources and whose value is still being realized.[9,10] By extracting valuable molecular constituents, macroalgae feedstocks can be transformed into a diverse array of bioproducts including food, biofuels, cosmetics, pharmaceuticals, materials, and other important goods.[11–14] For example, some species of red and brown macroalgae contain significant amounts of long-chain polyunsaturated fatty acids that could be used for nutritional supplements or as an animal feed/aquafeed.[15] Others are composed of high concentrations of carbohydrates that can be used to produce significant quantities of bioethanol.[16] Certain algal proteins have even been isolated for utilization as dyes for milk products.[17]

In addition to growing interest in the use of macroalgal derivatives for novel bioproducts, whole algal cells and tissues have been utilized to create materials.[18–21] In this case, the compositional complexity and diversity of different algae species could pose challenges when considering commercial scalability and product consistency. However, utilizing whole algae, rather than isolating useful components, reduces expenditures associated with chemical and mechanical extraction procedures. Manufacturing using this paradigm, where whole algal feedstocks are converted directly to products, also improves throughput and reduces waste and therefore merits investigation despite complexity introduced by interspecies chemical and biological variation. Following this model, several recent studies have used whole algal biomatter to fabricate alternatives to petrochemical products.[22–25] Petrochemical-derived materials, like most plastics, adhesives, epoxies, *etc.*, are among the most widely utilized modern materials. Their utility, chemical versatility, cost-efficiency, and highly tunable performance resulted in a 190-fold growth in their annual production between 1950 and 2015.[26] However, the production, consumption, and disposal of petrochemical-derived materials contribute to significant greenhouse gas emissions and the accumulation of micro- and nanoplastics in global ecosystems and food chains.[27,28] Therefore, leveraging the environmental benefits of macroalgae aquaculture to supplant specific, harmful petrochemical materials could have a magnified positive societal impact.

Recently, our group has utilized whole algal biomatter to develop strong and degradable bioplastics.[24] By applying heat and pressure, *Limnospira platensis* (Spirulina) cells were self-bonded to form a compostable material that could be a suitable replacement for plastic products with short life cycles. In another work, we demonstrated that macroalgae can function as a dry adhesive in engineered wood (particleboards), substituting the prevailing synthetic petrochemical resins, like phenol–formaldehyde.[25] Upon the application of heat and pressure to a solid mixture of wood particles and *Ulva expansa* macroalgae, the latter functions as an adhesive that binds wood particles together to form a composite construction material with mechanical properties similar to commercial engineered wood panels and inherent flame retardancy. Replacing even a fraction of the petrochemicals used for packaging, consumer goods, or building materials using these technologies could significantly reduce harmful environmental outcomes, especially given the projected growth in plastic production.[26] Despite their potential, the development of high-performing algal-based biomaterials is limited by our understanding of the mechanisms governing self-bonding during thermomechanical processing. Initial efforts to illuminate biomatter transformations at elevated pressures and temperatures indicate that the macromolecular composition of biomatter plastics distinctly influences processability and mechanical properties.[29] However, the roles of macroalgal molecular constituents and their interactions in intact tissues and cells have not been studied directly. Additionally, little research, if any, has concentrated on the comparison and evaluation of local macroalgal tissues as feedstocks to replace petrochemical materials.[30]

Here we focus on four native, commercially available, and culturally important Hawaiian macroalgal species as feedstocks for bioplastics and dry adhesives for wood particleboards. *Ulva* sp., *Caulerpa lentillfera*, *Gracilaria parvispora*, and *Halymenia*

hawaiiana were sourced directly from Hawai'i and are used as a case study for local macroalgae utilization. We provide a thorough compositional characterization of each species, aiming to connect the findings to the physical properties of the resulting bioplastics and particleboards. The sustainability of the novel algal materials are also quantified using respiromentric measurements of biodegradation. This study builds upon our earlier work by applying previously developed thermomechanical transformation methods to several commercially important Hawaiian macroalgae and by comprehensively characterizing their macromolecular fractions in detail to investigate the impact of chemical composition on whole macroalgal biomatter products.

2 Materials and methods

2.1 Macroalgae collection and preprocessing

Three macroalgae species, *Halymenia hawaiiana* (Halymenia, HH), *Gracilaria parvispora* (Gracilaria, GP), and *Caulerpa lentillifera* (Caulerpa, CL), were sourced from Ocean Era, a mariculture company located in Kailua-Kona, Hawaii, and *Ulva* sp. (Ulva, US) was obtained from the Ānuenue Fisheries Research Center (O'ahu). Each of the macroalgae was collected fresh and thoroughly rinsed first with tap water and then ultrapure water (Elga Purelab Flex 2) to remove salts and other surface contaminants. After washing, macroalgae samples were partitioned into separate fractions for downstream analyses. About half of the frozen macroalgal biomass was reserved for moisture and ash determination, while the remaining portion was lyophilized to analyze carbohydrate, protein, lipid, carbon, hydrogen, and nitrogen content. The lyophilized macroalgae samples were also ground to a fine powder using a mortar and pestle under liquid nitrogen and stored in centrifuge tubes in a desiccator until further analysis. To fully break down the tough cell walls of macroalgae for macromolecular analyses, lyophilized and crushed samples were further pulverized using bead milling (Tissuelyser II, Qiagen).

2.2 Compositional analysis

2.2.1 Moisture and ash content determination. Moisture and ash contents were determined following modifications to standard methods and NREL's analytical procedure, respectively.[31,32] In brief, to determine moisture content, washed macroalgae were spun in a reticulated spinner until a constant weight, which was then taken as the fresh weight. In quintuplicate, algae were weighed to 1 gram each on pre-weighed aluminum foil trays and dried at 105 °C overnight. The samples were then placed under vacuum in a desiccator until cooled to room temperature. Each algal sample was then weighed again, and the loss on drying was taken as the moisture content.

To prepare samples for ash content analysis, the frozen macroalgae were dehydrated at 60 °C overnight until constant weights were obtained, and then crushed to a fine powder and sieved through a 250 μm mesh to obtain a relatively homogeneous powder with no large chunks. The ash content was determined using thermogravmetric analysis (TGA) on a Discovery 550 TGA from TA Instruments (New Castle, DE, USA). Approximately 5–10 mg of each species was placed in 100 μL platinum pans and first heated to 105 °C at a rate of 10 °C per minute. After a 20 minute isothermal hold, the temperature was increased to 250 °C at a rate of 10 °C per minute and held constant for 30 minutes. Finally, the temperature was increased to 575 °C at a rate of 10 °C per minute and held constant for 12 h. The ash content was taken as the residual wt% of the original weight, given that the weight had stabilized after 12 h. Measurements were performed in triplicate.

2.2.2 Carbohydrate content determination. The carbohydrate content of the macroalgae samples was quantified using a modified phenol–sulfuric acid method.[33] In brief, ≈10 mg of lyophilized and ground macroalgae powder was weighed into 15 mL centrifuge tubes. 0.5 mL of glacial acetic acid was added to each tube and the tubes were then incubated at 80 °C for 20 minutes to facilitate cell disruption. Subsequently, 10 mL of acetone was added to the tubes to remove pigments, and the mixture was vortexed vigorously for 1 min. The tubes were then centrifuged at 4000 rpm for 5 minutes at 20 °C, and the supernatant containing the pigment fraction was discarded. The decolorized algal samples were then hydrolyzed with 5 mL of 4 M trifluoroacetic acid (TFA) at 100 °C for 30 min, after which the tubes were immediately transferred to an ice bath to cool. 20 μL of each hydrolysate was transferred to new microtubes, along with 0.9 mL of coloring reagent (100 mL H_2SO_4, 50 mL Milli-Q water, 0.5 g phenol). The tubes were then vortexed thoroughly and incubated in a 100 °C water bath for 20 minutes to facilitate color development by way of furfural and hydroxymethylfurfural (degradation products of sugars) formation. After incubation, the tubes were cooled in an ice bath, and 300 μL samples from each tube were transferred to a 96-well plate for spectrophotometric analysis at 490 nm, corresponding to the peak absorbance values of furfural and hydroxymethylfurfural. Absorbance measurements were compared to a calibration curve created with varying concentrations of glucose, 0.000, 0.025, 0.125, 0.250, 0.500, 0.750, 1.000, 1.250, and 1.500 mg mL^{-1}, which were subjected to the same acid hydrolysis and color development treatment as the macroalgal samples. The absorbance values at each concentration were recorded, and plotted with glucose concentrations on the *x*-axis and absorbance values on the *y*-axis. A regression line was then fit through the points to obtain the R^2, slope, and *y*-intercept, which were used to calculate the carbohydrate concentrations in each sample.

2.2.3 Protein content determination. To measure protein content, ≈5 mg samples of freeze-dried macroalgae were weighed in microtubes, hydrolyzed in 200 μL of 24% (w/v) trichloroacetic acid (TCA), incubated in a water bath at 95 °C for 5 min, and allowed to cool to room temperature (RT).[34] Samples were diluted to 6% (w/v) with 600 μL of ultrapure water, centrifuged at 15 000 rcf for 20 minutes at 4 °C, and the supernatants were discarded. The resulting cellular pellets were resuspended in 0.5 mL of freshly prepared Lowry Reagent D, which was made fresh by mixing Lowry Reagents A (2% (w/v) Na_2CO_3 in 0.1 N NaOH), B (1% (w/v) NaK Tartrate

tetrahydrate), and C (0.5% (w/v) $CuSO_4 \cdot 5H_2O$ in water) in a 48 : 1 : 1 ratio. The Lowry Reagent D suspensions were vortexed every 10 minutes while incubated at 55 °C for 3 h, after which the samples were cooled to RT. To clarify and separate the protein-rich supernatant from the cellular debris, samples were centrifuged at 15 000 rcf for 20 min. In a 96-well plate, 25 μL of the supernatant from each sample were mixed with 200 μL BCA reagent for spectrophotometric analysis at 562 nm. Calibration curves were prepared for each assay using a bovine serum albumin (BSA) stock solution (200 mg mL^{-1}; Sigma P5369) at concentrations of 0.000, 0.025, 0.100, 0.250, 0.500, 0.750, 1.000, 1.500, and 2.000 mg mL^{-1}. Similar to the calibration curve for carbohydrates, a regression line was fit through the points to obtain the R^2, slope, and *y*-intercept to calculate protein concentrations in the extracted solution and weight percentages in the macroalgal samples.

2.2.4 Lipid content determination. Total lipid content was determined using a modified version of the Bligh and Dyer method.[35] In brief, 20–50 mg of freeze-dried, crushed biomass was weighed in 8 mL glass tubes with screw cap tops and Teflon linings. To this, 2 mL of a 1 : 2 : 0.1 mixture of methanol : chloroform : formic acid was added and then vortexed for 30 minutes at 1500 rpm. Next, 1 mL of a solution of 1 M KCl and 0.2 M H_3PO_4 were added to each tube and the tubes were vortexed for 3 minutes at 200 rpm. The aqueous and organic phases were then separated through centrifugation at 1500 rpm for 5 minutes. The top layer containing the aqueous phase was discarded, and the bottom layer containing the organic phase was pipetted into a fresh 8 mL glass tube. The previous steps were repeated twice more to ensure complete removal of lipids from the biomass, and then the tube containing the total organic phase was dried under nitrogen gas until a constant weight. The original mass of the tube was subtracted from the tube weight with the dried lipids to calculate the lipid weight. The lipid weight was divided by the weight of biomass used in each extraction to calculate the lipid content of the biomass.

2.2.5 Sulfate content determination. Sulfate concentrations were measured by the turbidimetric method following the protocol reported by Torres *et al.*[36] A barium chloride–gelatin reagent was prepared by adding 75 mg of gelatin (VWR, 97 062-618) to 25 mL of ultrapure water in a 50 mL centrifuge tube, and incubating at 80 °C for 10 minutes. Next, 250 mg of anhydrous barium chloride (ThermoFisher, 99.998% purity, metals basis) was added to the water–gelatin mixture, and vortexed briefly. Hydrolyzed and non-hydrolyzed samples were prepared for total and inorganic sulfate content measurements, respectively. For the hydrolyzed samples, ≈1 mg of ground and dry macroalgal biomass was added to a microtube with 250 μL of 0.5 M HCl, vortexed for 60 seconds, incubated in a dry bath at 105 °C for 3 hours, and then left to cool to room temperature (23 °C). Hydrolyzed samples were then centrifuged at 13 400 rcf for 15 minutes, and the supernatant was transferred to a clean microtube. Non-hydrolyzed samples were prepared by weighing 5 mg of ground and dry macroalgal biomass into a microtube with 500 μL of ultrapure water. The samples were vortexed briefly, centrifuged at 13 400 rcf for 15 minutes, and the supernatant was transferred to a clean microtube. Separately, a sulfate calibration curve was prepared by adding 591.6 mg of Na_2SO_4 to 40 mL of ultrapure water in a 50 mL centrifuge tube, obtaining a stock solution of 10 mg mL^{-1} SO_4^{2-} ion. A 9-point calibration curve was created with SO_4^{2-} concentrations of 0.00, 0.10, 0.20, 0.40, 0.50, 0.75, 1.00, 1.50, and 2.00 mg mL^{-1}. A microplate reader (Tecan, Switzerland) was used to mix and measure the absorbance of individual wells in a 96-well microplate. 140 μL of 0.5 M HCl was added to each well, along with 20 μL of a blank (0.5 M HCl), standard (Na_2SO_4), hydrolyzed, or non-hydrolyzed sample. The plate was mixed at 567 cpm (counts per minute) for 60 s at 3 mm amplitude; then absorbance was read in each well at 405 nm to measure the background. After the background reading at 405 nm, 40 μL of the barium chloride–gelatin reagent was added to each well, mixed again at 567 cpm, and incubated for 20 minutes at RT. The microplate was then mixed again, and re-read at 562 nm to measure the absorbance change. The absorbance values were corrected by subtracting the background (405 nm) from the second reading (562 nm), and the calibration curve was constructed by plotting the known sulfate ion concentrations (0–2 mg mL^{-1}) on the *x*-axis against the corrected absorbance on the *y*-axis. Linear regression was used to determine a line-of-best fit and thereby quantify the sulfate ion concentration in each macroalgae sample. The total and free (inorganic) sulfate percentages in individual samples were then calculated by dividing the sulfate ion concentration by the mass of biomass used. The organic sulfate (OS) percentage was calculated using the following equation:

$$\mathrm{OS} = (\mu_\mathrm{H} - \mu_\mathrm{N}) \pm \sqrt{{\sigma_\mathrm{H}}^2 + {\sigma_\mathrm{N}}^2}$$

where μ_H and σ_H are the mean and standard deviation of the hydrolyzed samples, and μ_N and σ_N are the mean and standard deviation of the non-hydrolyzed samples. Although the turbidimetric assay cannot distinguish between different types of sulfated compounds, *e.g.* sulfated glycolipids, and metabolites, like sulfoquinovosyl diacylglycerol and dimethylsulfoniopropionate, these occur in relatively minute quantities in tropical macroalgae (less than 2% of DW).[37,38] Thus, it is assumed that sulfated polysaccharides constitute the majority of the organic sulfates detected.

2.2.6 Elemental composition determination. Carbon, hydrogen, and nitrogen measurements were performed using an Exeter Analytical CE 440 Elemental Analyzer (Exeter, Chelmsford, MA, USA). Analyses were conducted in triplicate on dried and ground macroalgae using 1.5–3.0 mg of biomass for each sample.

X-ray fluorescence (XRF) measurements were conducted using a Bruker M4 Tornado (Bruker, Billerica, MA, USA) with a Rh anode tube on dried and ground macroalgae. At least four measurements were taken for each species and the results were averaged.

2.2.7 Statistical analysis. Statistical analyses were conducted using *R* (version 4.4.2) and the packages dplyr (version 1.1.3), ggplot2 (version 3.5.1), multcompView (version 0.1–10), and tidyr (version 1.3.1). ANOVAs (analyses of variance) were conducted between macroalgae samples, and Tukey's HSD (honest significant differences) was used to compare group means.

2.3 Biomolecule characterization

2.3.1 High-performance anionic exchange chromatography (HPAEC). Macroalgae samples were subjected to acid hydrolysis prior to HPAEC. Samples were hydrolyzed using the methods reported by Wychen and co-workers.[39] Freeze-dried algae samples (25 mg) were weighed into 20 mL heavy wall glass pressure vessel tubes (Synthware, product #P160701). To these tubes, 250 μL of 72% (w/w) sulfuric acid solution (Fisher Scientific, CAS 7664-93-90, Waltham, MA, USA) was added and the contents were immediately vortexed. The tubes were incubated in a Reacti-Therm™ (made by Pierce, now Thermo Fisher Scientific, Waltham, MA, USA) at 30 °C for one hour, vortexing every five minutes. After incubation, the tubes were removed from the Reacti-Therm™ and 7 mL of Milli-Q water was added to each tube, reducing the sulfuric acid concentration to 4% (w/w). The tubes were placed back into the Reacti-Therm™ and incubated for one hour at 121 °C. After incubation, the tubes were removed and allowed to cool for one hour. The hydrolysate was then neutralized using small additions of calcium carbonate (Sigma-Aldrich, CAS 471-34-1, Saint Louis, MO, USA) until a neutral pH was achieved.

To separate the hydrolysate from acid-insoluble particulates, each tube was centrifuged at 8000 rcf for 15 minutes. The hydrolysate was removed and placed into a new 50 mL centrifuge tube. The hydrolysate was then neutralized again using small additions of calcium carbonate until a neutral pH was achieved. Neutralization reactions produced salts which precipitated from the hydrolysate solution. These salts were removed by an additional 15 minutes of centrifugation at 8000 rcf. The supernatant was removed and filtered using a 0.1 μm polyethersulfone (PES) syringe filter (J.T. Baker, Radnor, PA, USA). The filtered supernatant was placed into a new centrifuge tube and freeze-dried overnight. The freeze-dried samples were reconstituted in 1 mL of Milli-Q and placed into HPLC vials for HPAEC-PAD analysis.

Monosaccharide composition of each alga was determined using HPAEC with pulsed amperometric detection (HPAEC-PAD) on a Dionex ICS-6000 system equipped with dual eluent generators (Thermo Fisher Scientific, Sunnyvale, CA, USA), a CarboPac PA1 analytical column (1 × 250 mm), and a corresponding guard column (1 × 50 mm) (Thermo Fisher Scientific, Sunnyvale, CA, USA) that was maintained at a constant temperature of 30 °C. A 0.4 μL injection volume was used for all analyses. Each sample was diluted with Milli-Q water in a 1 : 2 ratio prior to injection.

Neutral monosaccharides and uronic acids were separated using a gradient of potassium methanesulfonic acid (KMSA) and potassium hydroxide (KOH) at a constant flow rate of 0.063 mL min^{-1}. The eluent gradient began with 0 mM KMSA and 15 mM KOH for 0.0–10.0 minutes, followed by 50 mM KMSA and 15 mM KOH between 10.1 and 25.0 minutes. From 25.1 to 40.0 minutes, the column was cleaned with 100 mM KMSA and 100 mM KOH, after which the system was re-equilibrated with 0 mM KMSA and 15 mM KOH from 40.1 to 60.0 minutes. Detection was performed using the standard quadruple-potential waveform for carbohydrates recommended by the manufacturer.

Monosaccharides were identified by comparison of retention times with authentic standards (Table S3) and quantified using calibration curves prepared from known concentrations of standards (10 sugars shown in Fig. S1). Specifically, six neutral sugar standards (rhamnose, arabinose, galactose, glucose, mannose, and xylose) and four uronic acid standards (galacturonic acid, guluronic acid, glucuronic acid, and mannuronic acid) were used to interpret the algal chromatograms. With the exception of two sugar pairs, the average peak positions and widths of the standard elution profiles are distinct and can be easily matched with the algal peaks. One exception is galacturonic acid and guluronic acid; the retention of these sugars overlaps. However, none of the algae contained appreciable concentrations of either of these monosaccharides, and so their superposition does not impact peak identification. Mannose and xylose also coelute, inhibiting the discrete assignment of peaks occurring at retention time ≈6 minutes. Despite this overlap, each peak was assigned to a sugar based on the location of maximum elution for ease of tabulation. As such, it is cautioned that the values reported for mannose and xylose in the following analyses may be convoluted.

2.3.2 Sodium dodecyl sulfate polyacrylamide gel electrophoresis (SDS-PAGE). SDS-PAGE was performed based on a method by Niu and co-workers.[40] 200 mg of macroalgae powder was suspended in 1 mL of lysis buffer composed of 50 mM Tris–HCl (pH 7.5), 150 mM NaCl, 2% (w/v) SDS, 1 mM EDTA, and a protease inhibitor cocktail (Sigma-Aldrich, P8849). The mixtures were homogenized by vortexing and incubated on ice for 60 minutes with intermittent mixing. Following extraction, samples were centrifuged at 13 400 rcf for 20 minutes at 4 °C, and the supernatant containing soluble proteins was collected and transferred to a new microtube. Proteins were precipitated by adding 1 mL of 10% (w/v) TCA to the supernatant, followed by incubation on ice for 30–60 minutes. The precipitated proteins were pelleted by centrifugation at 13 400 rcf for 15 minutes at 4 °C, and the supernatant was discarded. The pellet was washed with 500 μL to 1 mL of ice-cold acetone, briefly vortexed, and centrifuged at 13 400 rcf for 5 minutes. This washing step was repeated one to two times to remove residual TCA, SDS, and salts, and then the pellet was air-dried at RT for 5 minutes, and resuspended in 1× Laemmli buffer. Samples were then heated at 95 °C for 5 minutes to denature proteins and centrifuged briefly. Finally, 20 μL aliquots of each sample were loaded onto a 12% polyacrylamide gel for SDS-PAGE. Samples were run at 80 V for approximately 60 minutes until the dye front reached the end of the gel. The SDS gel was then incubated in a colloidal Coomassie solution (Coomassie Brilliant Blue G-250, 0.12% (w/v), phosphoric acid 2% (v/v), ammonium sulfate 10% (w/v), and methanol 20% (v/v)) and shaken gently overnight at RT in the dark to stain the protein bands. The background was removed from the gel by several washes using ultrapure water under gentle shaking and the finished gels were photographed to record the positions of the protein bands.

2.3.3 Gas chromatography with flame ionization detection (GC-FID). In preparation for gas chromatography with flame ionization detection (GC-FID), the previously extracted lipid

fractions were transesterified to obtain the corresponding fatty acid methyl esters (FAMEs).[41] 1 mL of fresh hexane was added to resolubilize the lipid fractions and 100 μL of each sample was transferred to clean glass tubes with PTFE-lined screw caps. 5 μg of tridecanoic acid (C13:0) was added to each sample as an internal standard. 1 mL of 1 M methanolic HCl was added to each tube and the solutions were heated at 80 °C for 25 minutes, and then immediately cooled to RT in a water bath. Equal 1 mL volumes of hexane and 0.9% (w/v) NaCl were then added to each sample. The samples were vortexed briefly, and then centrifuged at 1500 rpm for 5 minutes. The resulting upper phase was removed and collected in a clean glass tube, and dried under nitrogen gas. The samples were then resuspended in 100 μL of fresh hexane, transferred to GC vials, and subsequently run on an Agilent 8860 GC (Agilent, Santa Clara, CA, USA) equipped with an Agilent DB-23 column. The oven was initially set to 180 °C before ramping to 240 °C at a rate of 10 °C per minute, and held at 240 °C for 5 minutes. Individual saturated and unsaturated FAMEs were identified in Agilent OpenLab software by comparison of the macroalgal chromatograms to the retention times of a standard FAME mix (Supelco 37 Component FAME Mix). Concentrations of individual FAMEs were obtained by comparison of peak areas to the area of the internal C13:0 standard in each sample.

2.4 Bioplastic fabrication

Dried and ground macroalgae powders were stored at 40% relative humidity for at least one week before bioplastic fabrication. Bioplastic samples were made by loading 1 gram of humidity-equilibrated algae powder into a custom stainless steel mold described previously.[24] The stainless steel mold was then loaded into a TMAX-SYP-600 hot press (TMAXCN (China)) and hot-pressed for 5 minutes using one of four combinations of temperature and pressure derived from successful conditions in previous studies: (1) 140 °C and 7 kN, (2) 140 °C and 15 kN, (3) 160 °C and 7 kN, or (4) 160 °C and 15 kN[24,25]. The gap between the top and bottom of the press is incrementally reduced to account for powder compaction such that the pressure experienced by the specimen is constant during the duration of fabrication. After successful pressing, the mass and volume of each sample are measured and the apparent density is calculated.

2.5 Particleboard fabrication

The University of Washington wood shop provided raw sawdust from Douglas fir (*Pseudotsuga menziesii*). The sawdust was passed through a 150 μm mesh sieve to produce a wood flour free of large irregularities or contaminants. Algal powders were added to the sieved wood flour to create powder mixtures with 40 wt% algal powder. The 60–40 wt% wood–algae powders were vortexed and stored at 40% relative humidity for at least one week. The algae-bound particleboards were then fabricated using the same method described for the pure algal bioplastics.

2.6 Scanning electron microscopy

Specimens were prepared for scanning electron microscopy (SEM) by first applying a 4 nm gold coating using a 108 Manual sputter coater from Ted Pella. The sputtered samples were imaged using a Phenom ProX Desktop SEM (Thermo Fisher Scientific) with an accelerating voltage of 10 kV.

2.7 Mechanical testing

Before mechanical testing, algal bioplastic and wood–algae composite samples were stored in a desiccator for at least 24 hours. The flexural properties of the specimens were evaluated using an Autograph AGS-X Universal Precision Tester from Shimadzu Scientific Instruments outfitted with a 500 N load cell. $N = 6$ samples of each material were tested in three-point bending across a 40 mm span using a strain rate of 0.5% s^{-1}.

2.8 Sea water biodegradation measurement

To measure the biodegradation of macroalgal biomaterials, 1 g doses of ground specimens were added to sealed reaction vessels containing natural sea water inoculum prepared in accordance with ASTM D6691.[42] Sea water for these experiments was collected from Elliot Bay near Seattle, WA and was provided by the Seattle Aquarium. The sea water inoculum was prepared by adding 0.5 g L^{-1} and 0.1 g L^{-1} of NH_4Cl and $KH_2(PO_4)$ respectively. The total volume of inoculum added to each reaction vessel was 500 mL. CO_2 scrubbing chambers containing 100 mL of 3 M NaOH solution were attached to each vessel before each closed loop system was connected to an oxygen bag. The oxygen consumption over time was monitored using a BPC Blue closed-loop respirometer apparatus (BPC Instruments, Lund, Sweden). Both microcrystalline cellulose and blank reaction vessels were used as references. All measurements were performed in triplicate.

Using the respirometer system, the biochemical oxygen demand of each reaction vessel (BOD_t) was measured and reported in mg of oxygen. The approximate percentage of biodegradation (D_t) was calculated in accordance with ISO 14851 (ref. 43) using eqn (1), where BOD_s is the specific biochemical oxygen demand and ThOD is the theoretical oxygen demand. BOD_s (mg g^{-1}) is calculated using BOD_t (mg L^{-1}) by subtracting the BOD of the blank vessels and normalizing by the mass of sample per volume of inoculum (g L^{-1}). The ThOD of biomass is calculated here based on the procedure in ISO 14851 for the ThOD calculation of composite materials[43] and loosely on the work of Pupulawaththa.[44] First, the ThODs of each molecular constituent of biomaterials ($ThOD_i$) were individually calculated using eqn (2) assuming that all nitrogen undergoes nitrification during degradation. The molecular composition of the produced biomaterials was estimated to the fullest extent possible using both literature and experiments performed herein. The overall ThOD for each material was calculated by summing the product of the individual ThODs ($ThOD_i$) and their corresponding weight fraction for each component (X_i) as indicated by eqn (3). The complete composition and M_r values used to calculate ThOD of each material are included in Tables S1 and S2.

$$D_t = \frac{BOD_s}{ThOD} \times 100 \quad (1)$$

$$\mathrm{ThOD} = \frac{16[2c + 0.5h + 2.5n + 3s - o]}{M_r} \quad (2)$$

$$\mathrm{ThOD}_{\mathrm{total}} = \sum \mathrm{ThOD}_i \mathrm{X}_i \quad (3)$$

2.9 Flammability assessment

The flame resistance of the 60–40 wt% wood–algae composites was evaluated using $n = 4$ specimens for each material and a modified UL94-HB setup. 3 cm test coupons, held at one end by a pair of metal tweezers, were placed within the flame of a lit Bunsen burner for 10 s before being completely withdrawn. The time after withdrawal until the complete extinction of the burning specimen was recorded. It was noted whether or not each specimen self-extinguished before being entirely consumed.

2.10 Particle size measurement

To determine the particle size distribution of macroalgae powders, small amounts of each algae were suspended in water and imaged using a Motic Panthera TEC-BF (Motic, Kowloon Bay, Hong Kong). Images of the algae powders were taken using a 5× objective lens and individual particles were measured with the Fiji platform.[45] The size of a particle was determined as the average of two Feret's diameters. The first diameter was taken in the direction of the longest dimension of the particle and the second was measured approximately perpendicularly to the first.

3 Results and discussion

3.1 Physiology and compositional profiles of macroalgae

Four species of native Hawaiian macroalgae with varying physiology and composition were evaluated as potential feedstocks for biomaterials. Two species were chosen from phylum Chlorophyta (Caulerpa and Ulva) and two from phylum Rhodophyta (Gracilaria and Halymenia). These four species were chosen to facilitate comparisons both between and within different phyla. Starting from physiology, the microscopic observations of each species reveal significant differences in anatomy, even between the two green and two red algae (Fig. 1a). Caulerpa, also known as sea grapes, shown in Fig. 1ai and ii, is one of the biggest single-celled organisms in the world. It has a siphonous body plan with cytoplasm circulating throughout its rhizoids, fronds, and bubble-like ramuli (Fig. 1ai). Ulva, or sea lettuce, is commonly found along the rocky intertidal zone and often forms large green tides when conditions are favorable for their growth and reproduction. Unlike Caulerpa, Ulva does not have rhizoids or fronds and is instead composed of a two-cell thick, blade-like thallus which can be heavily ridged (Fig. 1aiii and iv). While the Chlorophyta studied here have significantly different physiologies, the two Rhodophyta are relatively similar. Gracilaria has irregular cylindrical branches that form from the main thallus, resulting in a bushy appearance (Fig. 1av). The cellular structure of Gracilaria is compartmentalized into outer cortex cells, and inner medulla cells (Fig. 1avi). Halymenia is a fleshy, gelatinous red macroalga that has a large central thallus with smaller thalli branching out (Fig. 1avii). Halymenia has a vibrant red coloration and, like Gracilaria, has outer cortex cells and inner medulla cells (Fig. 1aviii).

To understand how the underlying molecular composition of macroalgae could impact the utilization of whole algal tissues for bioplastics and biocomposites, the carbohydrate, protein, lipid, and ash contents of each of the four species were measured. In general, the approximate biomolecular composition of each phylum has been previously reported in the literature.[46–50] Green macroalgae have high concentrations of carbohydrates (23–56% of dry weight (DW)), moderate protein levels (3.5–25% DW), low lipid content (0.3–6% DW), and variable ash concentrations (12–78% DW).[49] Red macroalgae have slightly higher carbohydrate concentrations (38–77% DW), similar protein concentrations (4–24% DW), lower lipid concentrations (0.2–1.5% DW), and similar ash contents (11–56% DW).[50] And while the compositional ranges of each molecular class are reported for the different phyla, it is important to measure the exact composition of the four specific species harvested and used in this study to make accurate comparisons between the resulting materials. As such, the precise compositions of Caulerpa, Gracilaria, Halymenia, and Ulva studied herein were quantified (Fig. 1b). Statistical comparisons calculated using ANOVA and Tukey HSD are overlaid on Fig. 1b where different letters for the same macromolecular class indicate statistically different compositions. The carbohydrate concentration measured for the four species varies between 57 and 69% DW (Fig. 1b). Although there are no statistically significant differences between macroalgal carbohydrate compositions, there are two groups that appear distinct. Caulerpa and Halymenia (68.7 ± 5.6% of DW and 68.0 ± 4.6% of DW, respectively) have the highest carbohydrate content, followed by Ulva (58.6 ± 7.2% of DW) and Gracilaria (57.6 ± 1.9% of DW). Conversely, there are three statistically unique protein concentrations: Halymenia has the highest protein content overall at 11.9 ± 1.7%, followed by Ulva (8.7 ± 2.6% DW), Gracilaria (7.5 ± 1.1% DW), and Caulerpa (5.2 ± 1.7% DW). The lipid contents vary between 2 and 11% of DW for the algae, with two statistically significant groups. Caulerpa has the highest lipid content at 10.4 ± 2.2% DW, followed by Halymenia (4.6 ± 1.5%, Gracilaria (2.5 ± 0.9% DW) and Ulva (2.3 ± 0.5% DW). Lastly, ash concentrations range between 24 and 47% DW. Each macroalgae has a statistically significant ash concentration, with Gracilaria having the highest (46.9 ± 1.7% DW), followed by Caulerpa (42.9 ± 1.2% DW), Ulva (31.6 ± 1.5% DW), and Halymenia (24.6 ± 1.0% DW). Overall, the molecular compositions measured for each of the four species fall within ranges previously reported.[49,50]

3.2 Characterization of macroalgal biomolecules

Each of the four species of macroalgae analyzed here is principally composed of carbohydrates. Specifically, macroalgae are known to contain significant amounts of polysaccharides with sulfated functional groups (*e.g.*, ulvans, carrageenan, agar, and

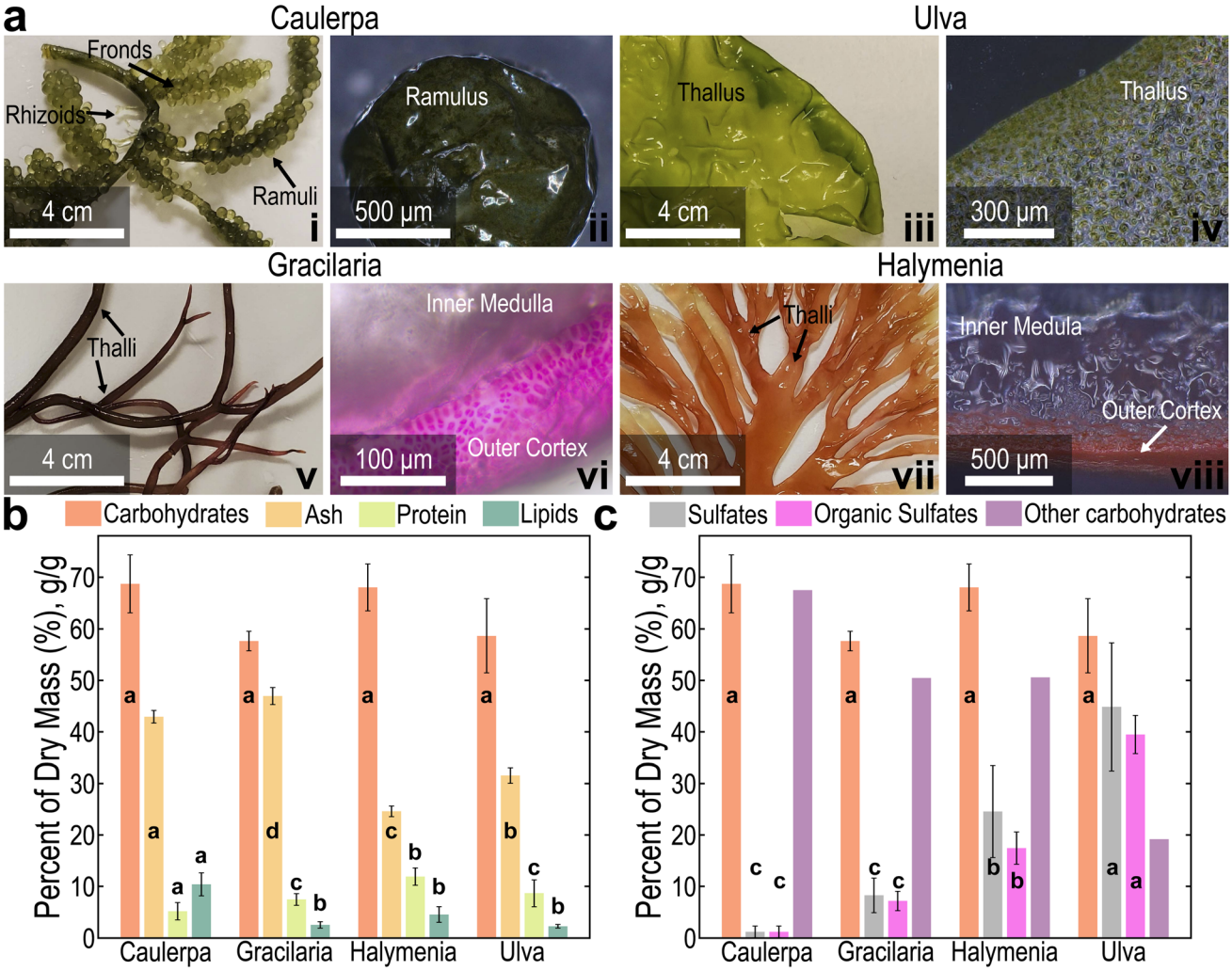

Fig. 1 (a) Digital images of the macro- and microscopic morphology of (i) and (ii) Caulerpa, (iii) and (iv) Ulva, (v) and (vi) Gracilaria, and (vii) and (viii) Halymenia. (b) The carbohydrate, ash, protein and lipid content in the four algal species represented as the percentage of dry weight (DW). (c) The content of carbohydrates, sulfates, organic sulfates, and non-sulfated carbohydrates present in each of the four algal species as a percentage of the DW. The percentage of 'Other Carbohydrates' is calculated as the difference between total carbohydrates and organic sulfates. Where present, error bars indicate ±1 standard deviation. Data without error bars are calculated rather than measured. The letters overlaid over each bar in subfigures (b) and (c) indicate statistically distinct groups as calculated using ANOVA followed by Tukey HSD (significance level = 0.05).

fucoidans).[51] Measurements of the concentrations of total sulfates and organic sulfates are presented in Fig. 1c, and three statistically significant groups (marked with letters a, b, c) are distinguished. Ulva had the highest concentration of total sulfates at 40.3 ± 7.4% DW, followed by Halymenia at 23.2 ± 5.8% DW, and then Gracilaria and Caulerpa at 6.6 ± 3.3% DW and 1.2 ± 1.1% DW, respectively. The organic sulfate contents were calculated to be 34.9 ± 7.5%, 16.2 ± 5.8%, 6.6 ± 3.3%, and 1.2 ± 1.1% for Ulva, Halymenia, Gracilaria, and Caulerpa, respectively. Because inorganic sulfates in Gracilaria or Caulerpa were not detected, it was assumed that the entirety of the sulfates detected were organic sulfates.

To study the polysaccharide content of each species in greater detail, carbohydrates were extracted, hydrolyzed, and analyzed using HPAEC-PAD (Fig. 2a and b). The results indicate that the two Chlorophyta species (Caulerpa and Ulva) have relatively dissimilar monosaccharide contents. Caulerpa has a relatively high concentration of mannose/xylose (2.79% DW) and moderate concentrations of galactose (0.45% DW) and glucose (0.49% DW) (Fig. 2b). Caulerpa does not contain significant concentrations of uronic acids. The monosaccharide content of Ulva, on the other hand, is composed of glucose (1.85% DW), glucuronic acid (1.74% DW), rhamnose (0.97% DW), and xylose/mannose (0.42% DW). The detection of these monosaccharides corresponds to the sulfated polysaccharides that have been previously isolated from Caulerpa and Ulva. Sun *et al.* extracted sulfated xylogalactomanans from Caulerpa with similar monosaccharide compositions to measurements obtained in this study (Fig. 2b).[52] The polysaccharides had high concentrations of mannose, galactose, and xylose and a sulfate content varying from 0–21%. The variable sulfate content of xylogalactomannans reported[52] may explain the relatively low

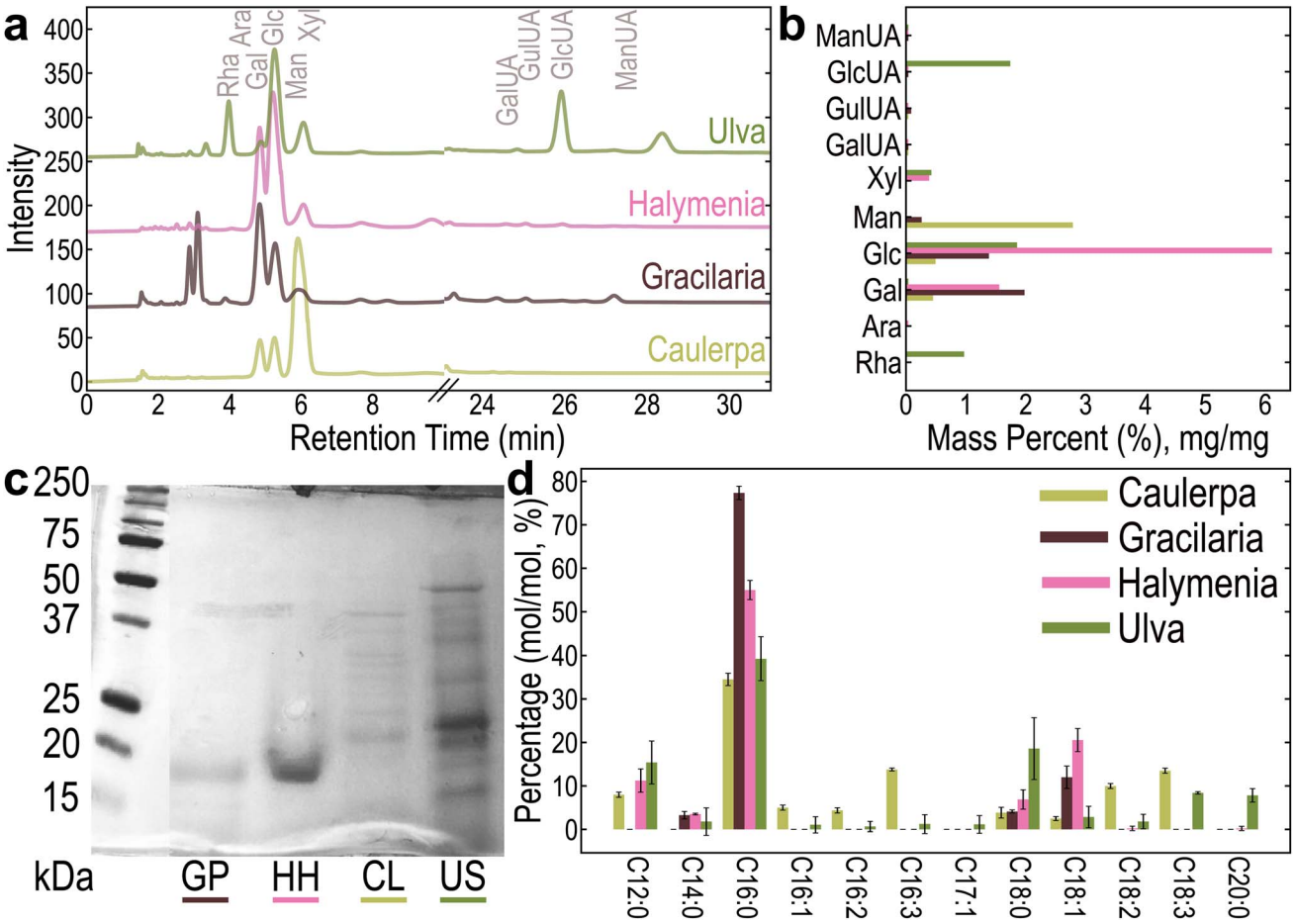

Fig. 2 (a) Chromatograms and (b) the concentration of different monosaccharides in macroalgae measured using HPAEC-PAD. The specific monosaccharides quantified are rhamnose (Rha), arabinose (Ara), galactose (Gal), glucose (Glc), mannose (Man), xylose (Xyl), galacturonic acid (GalUA), guluronic acid (GulUA), glucuronic acid (GlcUA), and mannuronic acid (ManUA). (c) An image of protein bands in an SDS-PAGE gel after extraction from Gracilaria (GP), Halymenia (HH), Caulerpa (CL), and Ulva (US). The bands measured for the macroalgae are compared to a ladder of standard proteins with molecular weights between 15 and 250 kDa. (d) The concentration of specific fatty acids in the total lipid composition extracted from Hawaiian macroalgae measured with GC-FID. Error bars in (d) indicate ±1 standard deviation.

concentration of sulfates measured for Caulerpa (Fig. 1c). Xylans have also previously been extracted from Caulerpa[53] and the glucose detected could have originated from starch. Instead of the mannose and galactose dominated polysaccharides found in Caulerpa, the principal sulfated polysaccharides in Ulva (ulvans) are primarily composed of rhamnose, glucuronic acid, and xylose.[54] Detection of these sugars (Fig. 2b) and a high concentration of sulfates (40.3% in Fig. 1c) suggest that the polysaccharide content of Ulva is dominated by ulvans. In addition to ulvans, cellulose, a neutral polysaccharidic glucosan, has also been isolated from Ulva.[55] Unlike the Chlorophyta, the Rhodophyta studied here (Halymenia and Gracilaria) have similar monosaccharide compositions; both contain relatively high concentrations of galactose and glucose, lower concentrations of xylose/mannose, and insignificant concentrations of uronic acids (Fig. 2b). The high concentrations of galactose in these red algae are attributable to the presence of agar and carrageenan.[56] While the HPAEC-PAD results indicate that both Gracilaria and Halymenia have similar galactose concentrations, prior studies suggest that the galactans in Gracilaria are predominantly agarans[57,58] and those in Halymenia are similar to λ-carrageenans.[59] The turbidimetric measurements in Fig. 1c support this conclusion; carrageenan has a higher sulfate density than agar[56] and Halymenia has a higher sulfate concentration than Gracilaria despite similar galactose contents. In addition to these galactans, the glucose detected in the Rhodophyta samples suggests that they may contain Floridean starch or small concentrations of cellulose.[60,61]

Overall, the monosaccharides identified using HPAEC-PAD largely agree with prior studies of the four macroalgae. However, some peaks could not be identified and the total concentrations of monosaccharides measured fall well below the carbohydrate contents determined using the phenol–sulfuric acid method. The most prominent unidentified peaks occur between 2.8 and 3.1 minutes in the Gracilaria chromatogram and have areas exceeding all identified sugars except galactose and glucose. These peaks do not match the locations

of any standards represented in Table S3. Based on the rapid elution of the two populations (≈2.876 and 3.101 min), it is possible that the peaks could be attributed to fucose[58] or similar deoxyhexoses with lower molar mass. The low overall detection of total monosaccharides, on the other hand, could be explained by incomplete hydrolysis of algal polysaccharides. However, while the polysaccharides may not have been completely depolymerized, it was assumed that they hydrolyzed proportionally such that the monosaccharide profile observed from HPAEC-PAD is representative of the total carbohydrate contents of each species.

In addition to the polysaccharide contents, the protein contents of the four macroalgae were also characterized more closely, using SDS-PAGE (Fig. 2c). The separation indicates that the green and red algae contain contrasting protein fractions. The green algae protein isolates comprise many distinct groups with molecular weights varying between 15 and 75 kDa. The identity of specific proteins in Caulerpa and Ulva has not been thoroughly characterized in the literature; however, previous SDS-PAGE results have shown proteins within the range of 6.5 to 116 kDa for Caulerpa, and between 11 and 110 kDa for Ulva.[62,63] Unlike the green macroalgae, the protein contents of the two red species formed a single band between 15 and 20 kDa, which may correspond to phycoerythrin subunits. Previous work has demonstrated the presence of multiple subunits that make up the phycoerythrin complex in Gracilaria and Halymenia, with molecular weights varying from 18–27 kDa and 16–47 kDa, respectively, matching the bands that were observed.[64,65] Prior research also indicates that both Gracilaria and Halymenia contain proteins other than those indicated on the gel in Fig. 2c. However, these additional proteins were not observed, possibly as a result of species-level compositional differences or of compositional differences induced by varying cultivation conditions.

To more carefully examine the lipid fractions of each of the Hawaiian macroalgae, GC-FID was employed to identify individual fatty acids. The relative concentration of individual fatty acids between C12:0 and C20:0 detected in the total lipid contents of the four species is presented in Fig. 2d. Caulerpa has the most distinct fatty acid profile measured, being composed of 49% saturated, 7.5% monounsaturated, and 43.5% polyunsaturated fatty acids (% of total lipids, mol mol^{-1}). The other species analyzed have, on average, much higher saturated fatty acid content (77–85%), and relatively lower monounsaturated (5–20.5%) and polyunsaturated (2.6–12.1%) fatty acid content. The dominant fatty acid among the macroalgae is palmitic acid (C16:0), with concentrations ranging between 34.5 and 77.3% (% of total fatty acids). This is typical among macroalgae; palmitic acid is generally the most abundant fatty acid among the three main macroalgae phyla.[66] Notably, the two red macroalgae have substantial amounts of monousaturated fatty acids (MUFAs). Specifically, Halymenia and Gracilaria have 20.5% and 11.9% oleic acid (C18:1) respectively. Contrarily, the green macroalgae have greater concentrations of polyunsaturated fatty acids (PUFAs), such as hexadecadienoic (C16:2), hexadecatrienoic (C16:3), and linolenic (C18:3) acids. The differences in the fatty acid profiles between the green and red Hawaiian macroalgae are likely due to their individual metabolisms and variations in environmental conditions during growth (*e.g.*, light, temperature, and nutrient availability). For example, green macroalgae utilize C16 PUFAs (C16:2, C16:3, and C16:4) to build thylakoid envelopes.[67] Additionally, the concentrations of C16:4 in Ulva and arachidonic acid (C20:4) and eicosapentaenoic acid (C20:5) in Halymenia and Gracilaria are lower than those previously reported.[50,61,68] The absence of these PUFAs has been associated with warmer cultivation temperatures, possibly because less unsaturated fatty acids are required to maintain cell membrane fluidity.[68,69]

Finally, while no further direct analyses of macroalgal ash content was performed here, XRF results can be utilized to infer ash composition (Table S4). The relatively high concentrations of chlorine, potassium, and sodium in the macroalgae are likely due to osmoregulation with their environment, causing the accumulation of salts within their cells. Other inorganic elements, like silica and metals present in the algal tissues, also likely contribute to high ash contents and could again be related to osmoregulation or diatomic colonies present on the surface of algal thalli.

Considered holistically, the biomolecular characteristics detailed here for the four macroalgae could be utilized to match each feedstock to desired bioproducts (*e.g.*, biodiesel/biofuels, nutraceuticals, *etc.*). For example, the low lipid concentrations (between 2 and 10%), and high moisture content (between 88 and 95%) of the four species may render biodiesel/biooil distillation economically infeasible.[70] On the other hand, the high carbohydrate concentrations (between 58 and 69%) and the presence of rare polysaccharides (*e.g.*, floridian starch, carageenan, and ulvan) suggest that carbohydrate extraction from these macroalgae could serve as an alternative source of bioethanol or therapeutic biopolymers. Ideally, individual extraction and processing steps could be combined into an integrated pathway to develop a biorefinery manufacturing paradigm and improve efficiency.[71] However, in practice, this is extremely complex and requires significant care to ensure that downstream processes are not impacted by previous steps. Alternatively, biomolecular extraction can be circumvented altogether if whole algal biomass is used to make useful bioproducts, as discussed in the following sections. In this case, macromolecular characterization can still serve an important role in comparing the aptitude of different algal species as biomaterial feedstocks and interpreting differences in material performance.

3.3 Mechanical and morphological characterization of macroalgae-based bioplastics

Each of the four species of macroalgae was successfully transformed into a bioplastic upon the application of heat and pressure (Fig. 3a). The dry, powdered algae were hot-pressed using four different conditions (Table S5) to account for the effects of varying processing parameters on the degree of self-bonding.[24] The mechanical performance of the resulting bioplastics was evaluated using three-point bending to identify the conditions that produced the most cohesive and robust

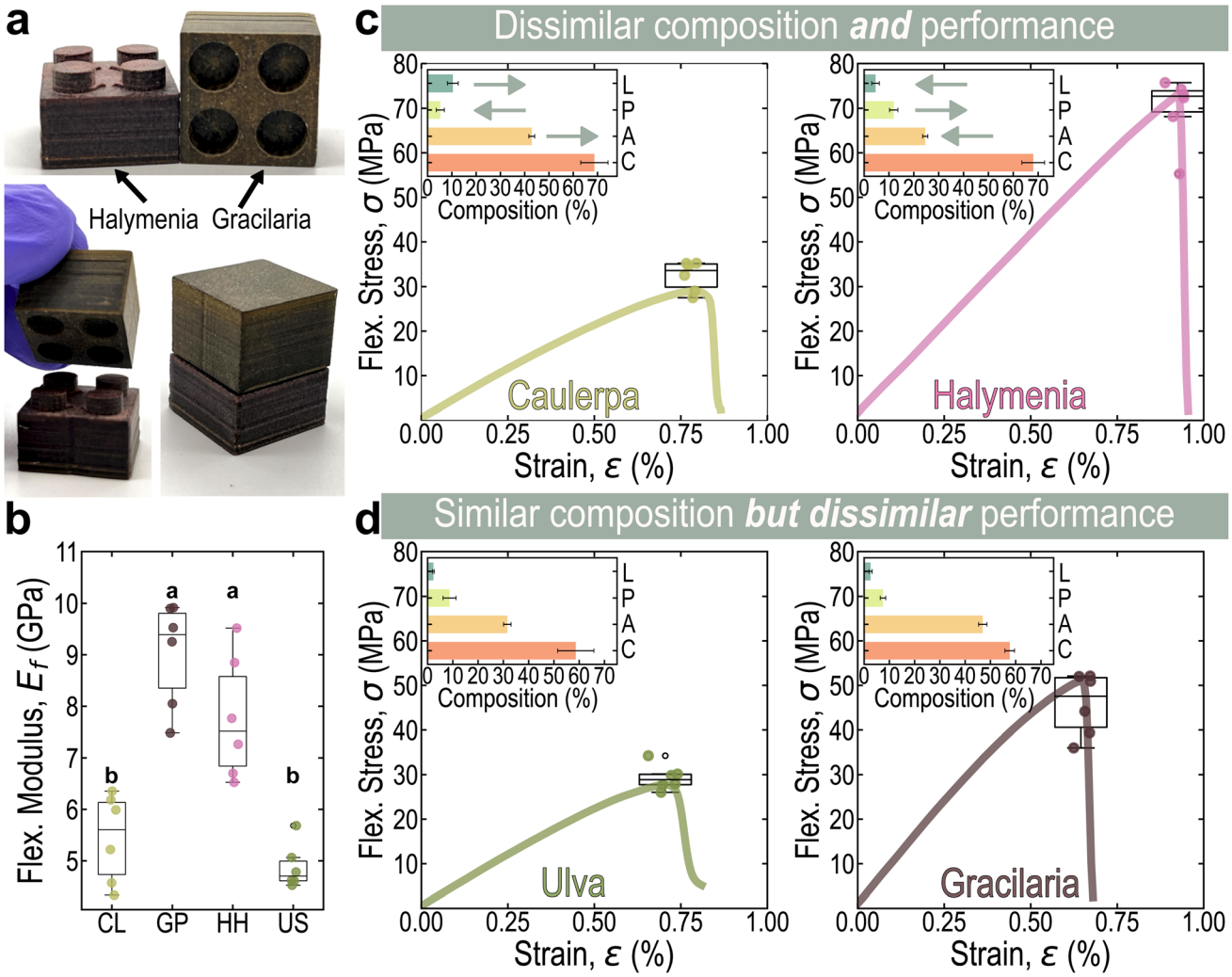

Fig. 3 (a) Photographs and (b) the flexural modulus of Hawaiian algal bioplastics. Lowercase letters signify distinct statistical groupings calculated using ANOVA and Tukey HSD (significance level 0.05). Representative flexural stress–strain curves and flexural strength data for pairs of algal species with (c) dissimilar and (d) similar composition, joined side by side for ease of comparison. The inset bar charts indicate the algal carbohydrate (red), protein (green), lipid (blue), and ash (orange) compositions expressed as % of DW. The error bars in these inset plots represent ±1 standard deviation. The populations compared in (c) and (d) are statistically distinct, as calculated using ANOVA and Tukey HSD as in (b). The box plots overlaid on scattered data in (b) and (c), and (d) demonstrate the upper and lower quartiles while the upper and lower whiskers represent ± 1.5 of the interquartile range respectively.

material for each species (Tables 1 and S5). Notably, the combination of temperature and pressure that resulted in the highest average flexural strength varied for the different algae. For example, the bioplastics made from Gracilaria exhibit a maximum average flexural strength of 45.8 ± 7.0 MPa after processing at 160 °C and 15 kN of pressing force while Ulva bioplastics have the highest average flexural strength of 29.3 ± 2.9 MPa after processing at 140 °C and 7 kN of pressing force (Table 1). Therefore the bioplastics with the highest flexural strengths for each species (conditions labeled as HFS), rather than the algal bioplastics formed under a single set of processing conditions, were compared in order to omit the influence of varying processability on the mechanical performance.

The maximum flexural modulus and strength obtained under the HFS conditions for each species, are summarized in Fig. 3b–d and Table 1. Halymenia demonstrates the highest flexural strength (69.8 ± 7.6 MPa) and flexibility (0.91% ± 0.11%) among the HFS bioplastics. Gracilaria demonstrates the highest average flexural modulus (9.0 ± 1.0 GPa), although its performance is statistically similar to the flexural modulus of Halymenia (7.8 ± 1.2 GPa). And while the flexural strength and modulus of these two red algae are distinctly superior to those of the green algae, all species impressively exceed 4 GPa flexural modulus and 29 MPa flexural strength (Fig. 3b–d). Additionally, all species, except Ulva, form bioplastics with similar apparent density (approximately 1.6 g cm^{-3}) (Table S5). In this regard, the mechanical performance of HFS seaweed bioplastics approaches or exceeds the flexural characteristics of commodity polymers and polymer composites, suggesting that these materials would be suitable to replace traditional plastics for some applications.[72–74] The SEM images of the HFS algal bioplastics shown in Fig. 4 demonstrate that in all cases, a matrix

Table 1 The carbohydrate, protein, lipid, ash, and moisture contents of Hawaiian algae, given as a percentage of dry mass, as well as the flexural modulus (Modulus), flexural strength (Strength), and strain-to-break (StB) of the bioplastic made from each species processed under a given condition. Superscripts (*a, b, c,* and *d*) indicate statistically similar/dissimilar groups calculated using ANOVA and Tukey HSD

Algae	Carbohydrate (%)	Protein (%)	Lipids (%)	Ash (%)	Moisture (%)	Condition[a]	Modulus (GPa)	Strength (MPa)	StB (%)
Caulerpa	68.7 ± 5.6^{a}	5.2 ± 1.7^{a}	10.4 ± 2.2^{a}	42.9 ± 1.2^{a}	95.3 ± 0.7	3	5.4 ± 0.9^{b}	32.4 ± 3.4^{c}	0.68 ± 0.07^{b}
Gracilaria	57.6 ± 1.9^{a}	7.5 ± 1.1^{c}	2.6 ± 0.6^{b}	46.9 ± 1.7^{d}	89.3 ± 0.3	4	9.0 ± 1.0^{a}	45.8 ± 7.0^{b}	0.58 ± 0.07^{b}
Halymenia	68.0 ± 4.6^{a}	11.9 ± 1.7^{b}	4.6 ± 1.5^{b}	24.6 ± 1.0^{c}	89.9 ± 5.0	4	7.8 ± 1.2^{a}	69.8 ± 7.6^{a}	0.91 ± 0.11^{a}
Ulva	58.6 ± 7.2^{a}	8.7 ± 2.6^{c}	2.3 ± 0.3^{b}	31.6 ± 1.5^{d}	88.1 ± 0.4	1	4.9 ± 0.4^{b}	29.3 ± 2.9^{c}	0.70 ± 0.05^{b}

[a] For each of the conditions 1–4 specimens are hot-pressed for 5 min at (1) 140 °C and 7 kN, (2) 140 °C and 15 kN, (3) 160 °C and 7 kN, or (4) 160 °C and 15 kN.

is formed that binds the constituent biomass together, resulting in a densified, continuous material. Heat and pressure applied during processing cause algal cells to partially disassociate and enable molecular interactions which cause self-bonding. The formation of a self-bonded matrix likely explains the flexural rigidity observed for the four algae.

Despite the formation of a cohesive matrix, the morphologies of the algal bioplastics are non-uniform. Pieces of whole algal tissue are visible, often bound within a homogeneous regime, as in the case of Caulerpa (Fig. 4a), or compressed into tight layers, as in the case of Halymenia (Fig. 4c). The presence of intact tissues suggests that the energy supplied during fabrication was not sufficient to fully disrupt cellular order and enable total homogenization. Visible tissue remnants, and the size analysis of algal powders in Fig. S3, also indicate that the lyophilization and grinding of the raw biomass did not produce a uniform feedstock. While most of the macroalgae powder is less than 75 μm in diameter, particles as large as 1.1 mm remain (Fig. S3). The Gracilaria and Halymenia powders in particular have a high frequency of particles larger than 350 μm in diameter. Previous findings demonstrated that pre-processing algal feedstocks to disrupt cellular structure can increase morphological uniformity and improve bioplastic flexural strength by 38%.[24] It follows that large tissue remnants would be detrimental to overall material performance; however, Halymenia and Gracilaria, under HFS conditions, exhibit the greatest flexural stiffness and strength among the species tested. In this regard, it is hypothesized that a balance of small particles may encourage molecular interaction and cohesion while intact tissues could act as structural reinforcement, resulting in optimal algal bioplastic performance. In addition, the larger particle size distribution causes a higher packing density during solid compaction, which could also enable the red macroalgae to form denser bioplastics than the green species.[75] Measurement of the apparent density of the bioplastics supports this assumption; the macroalgae with the narrowest particle size distribution (Ulva) also produce the bioplastics with the lowest density (1.46 ± 0.15 g cm^{-3}) (Table S5). Finally, SEM observations clearly show that diatoms and salt crystals are present throughout the algal biomatter, as indicated in Fig. S4 for Gracilaria and Caulerpa. Previous research has indicated that the introduction of small concentrations of inorganic fillers, specifically diatoms,[76] into a thermoplastic matrix could improve the composite stiffness and strength. While one would expect a similar mechanical reinforcement, especially as a result of favorable interactions between

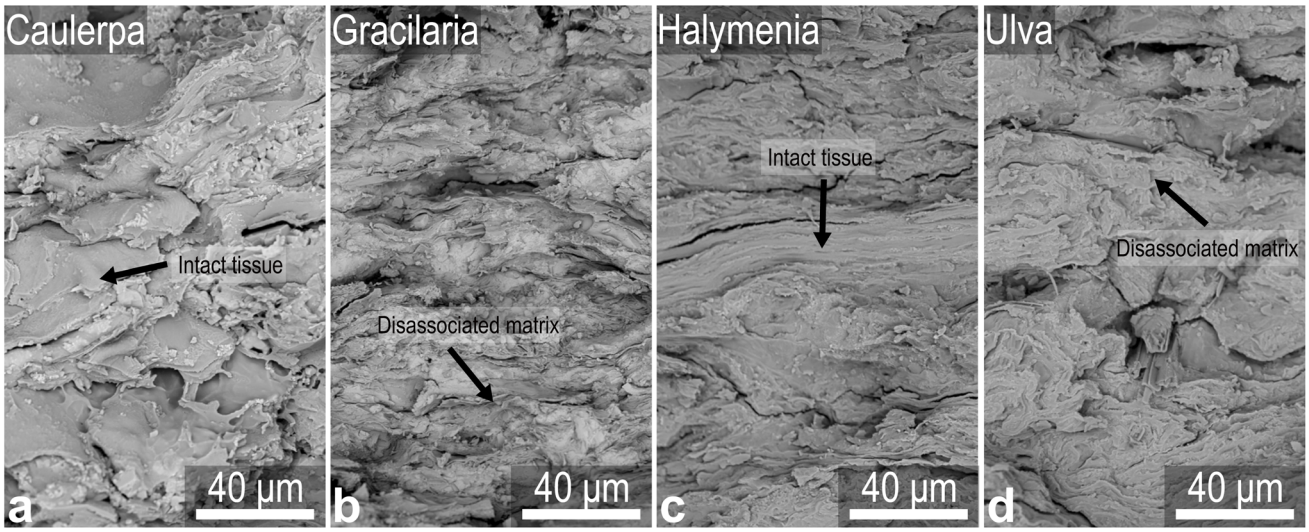

Fig. 4 SEM micrographs of (a) Caulerpa, (b) Gracilaria, (c) Halymenia, and (d) Ulva bioplastics fabricated using HFS processing conditions.

hydroxylated silicates on the diatom surface and biomatter, the macroalgal matrix does not flow to fill hollow areas within the diatomic skeletons, as a low viscosity polymer would (Fig. S4). As a result, the diatomic frustules behave more as voids than as reinforcing fillers. It is possible, therefore, that the diatoms, as well as the salts, within the biomatter matrix concentrate stress and create high energy interfaces, facilitating crack initiation and propagation, ultimately hindering mechanical performance. Further optimization of the washing and grinding of raw algae may optimize cellular disassociation and tissue reinforcement, remove inorganic contaminants, and augment bioplastic performance. In spite of these opportunities to improve macroalgal pretreatment, the HFS bioplastics exhibit impressive mechanical properties.

Aside from feedstock heterogeneity, differences in the manufacturability, mechanical performance, and morphology of the four algal bioplastics can also be attributed to variations in chemical composition and molecular characteristics. For example, while Halymenia and Caulerpa have similar carbohydrate compositions ($\approx$68%), Halymenia contains more than 2 times the protein and the two algae exhibit significantly different HFS properties (Fig. 3c). The flexural strength and stiffness of the HFS Halymenia are approximately 1.4 and 2 times greater, respectively, than those of the HFS Caulerpa (Fig. 3c and Table 1). Previous work demonstrated that protein aggregation during thermomechanical processing of a clean composite system played an important role in bioplastic cohesion.[29] In that model system it was concluded that molecular entanglement and changes in inter- and intramolecular hydrogen bonding likely caused the formation of a proteinaceous matrix, which encapsulated polysaccharide fibers. Insufficient protein content inhibited the development of a cohesive matrix and significantly diminished mechanical performance. It is possible, therefore, that the higher protein content in Halymenia contributes to a more uniform and cohesive matrix than Caulerpa, and therefore higher flexural strength and stiffness. The compositional bar-chart insets in Fig. 3c also show that Caulerpa has a significantly higher concentration of lipids than Halymenia (10% as opposed to 5%). It has been reported that fatty acids can serve as plasticizers and improve the flexibility of biomaterials by facilitating molecular mobility.[77] However, lipids, unlike proteins, have also been observed to have a deleterious effect on the mechanical performance of algal biomatter analogues. At 10% of total solid mass, mobile lipids self-associated and formed nanocrystals during thermomechanical processing rather than associating with other biomolecules.[29] Thus, the relatively high concentration of lipids in Caulerpa could enable the formation of microcrystalline defects and further hamper flexural performance compared to Halymenia. Finally, Caulerpa has a higher concentration of ash, or inorganic matter than Halymenia, as evidenced by large crystalline particles, likely salt, present in its microstructure (Fig. S4). While these inorganic defects may act similarly to lipid microcrystals to limit HFS Caulerpa's mechanical properties, prior work has also demonstrated that the addition of small concentrations of nanocrystalline fillers to algal bioplastics can provide structural reinforcement.[24] Nevertheless, the large concentration of ash in Caulerpa (42%) likely precludes reinforcement effects.

Unlike Halymenia and Caulerpa, comparing the concentrations of different classes of biomolecules does not explain the differences in flexural properties of Gracilaria and Ulva. Despite having remarkably similar nutrient compositions (approximately 58% carbohydrates, 8% proteins, and 2% lipids) (Fig. 3d), HFS Gracilaria has a flexural stiffness and strength approximately 2 and 1.65 times greater, respectively, than those of HFS Ulva. In this case, differences in the molecular characteristics of the two algae, rather than strictly the concentration of different macromolecular classes, may explain their varying mechanical properties. For example, the SDS-PAGE results indicate that Gracilaria has a high concentration of low molecular weight proteins, likely phycoerythrin subunits ($\sim$20 kDa),[78] and Ulva contains a variety of proteins with molecular weights ranging from 15 to 75 kDa (Fig. 2c). The size of different proteins affects their propensity to aggregate, in this case, at elevated temperatures in the solid state. In systems with relatively low protein concentration, like Gracilaria and Ulva, aggregation may be diffusion limited, where protein–protein interactions are dictated by the frequency of intermolecular collisions.[79] At elevated temperatures and pressures experienced during thermomechanical processing, the low molecular weight phycoerythrin subunits in Gracilaria likely diffuse more readily than higher molecular weight proteins in Ulva, leading to a higher occurrence of protein–protein interactions and aggregation. Therefore, as with Halymenia and Caulerpa, more extensive protein aggregation may explain the increased flexural strength and stiffness of HFS Gracilaria compared to HFS Ulva (Fig. 3b and d).

The sulfate content and monosaccharide constitution of the polysaccharides in each species may also affect the manufacturability and performance of the macroalgal bioplastics. However, unlike protein molecular weight, it is difficult to identify clear trends relating the sulfate content or HPAEC-PAD results to the mechanical properties. The macroalgae with the highest sulfate contents (Fig. 1c) form both the HFS bioplastics with the highest (Halymenia) and lowest (Ulva) flexural strength (Fig. 3c,d. Furthermore, while the turbidimetric sulfate assay (Fig. 1c) and HPAEC-PAD (Fig. 2b) results suggest that Halymenia is rich in sulfated carrageenans and Gracilaria is rich in agar, it is difficult to identify consistent findings in the literature to relate this trend to the differences in mechanical properties between the Rhodophyta. Studies of cast agar and carrageenan films find that carrageenan films have higher tensile strengths and lower elongation-to-break than cast agar films.[80,81] On the other hand, studies of carrageenan and agar gels feature mixed results. Rhein-Knudsen *et al.* demonstrated that carrageenan gels have higher storage moduli than agar gels[82] while Fuchs *et al.* showed that decreasing the sulfate content of carrageenan to form agarose like gels increased the storage modulus.[83] While it's possible that the presence of carrageenan rather than agar in Halymenia contributes to its higher flexural strength (52%), the film studies suggest that the agar rich material should have higher flexibility. The opposite was observed; Halymenia has a higher strain-to-break (56%) than Gracilaria. It is also unclear if these studies are relevant to the bulk macroalgal bioplastics

produced in this study. The form factors and concentrations of bound water differ and the effects of the carbohydrates on the macroalgae bioplastics may be convoluted by the effects of the protein, ash, and lipids discussed above. Additionally, the mechanical behavior of polysaccharides is influenced by their molecular weight and their hierarchical organization within the cellular physiology of algae.[84] As such, further studies are required to discern the impacts that different sulfated polysaccharides and polysaccharidic order have on the mechanical performance of whole algal bioplastics.

Taken together, analysis of biomolecular characteristics and micromorphology can be utilized to explain why algae with similar balances of each macromolecular class (Caulerpa *vs.* Halymenia and Ulva *vs.* Gracilaria) have different mechanical properties. Specifically, comparing Halymenia to Caulerpa validates the conclusions drawn during prior work;[29] all else equal, the species with higher protein content and lower lipid content had higher flexural strength. In fact, in both cases, comparing "like" species reveals that the red algae outperform the green algae. SDS PAGE results and particle size analyses demonstrate that the red species contain lower molecular weight proteins and larger particle size distributions, likely leading to increased cohesion, densification, and flexural performance. Differing sulfated polysaccharide compositions and hierarchical structural organization likely also influence macroalgal bioplastics, but additional studies are required to isolate and deconvolute their effects. Ultimately, combining analyses of molecular compositions and physical/morphological characteristics between algal species helps to infer the molecular transformations occurring during thermo-mechanical processing and to interpret differences in the resultant bioplastic micromorphology and mechanical properties.

3.4 Application of Hawaiian macroalgae as dry adhesives for particleboards

The thermoformability of Hawaiian algae was further leveraged to produce wood particleboards without the use of toxic flame-retardant additives and synthetic resins such as phenol–formaldehyde.[85] Heated compression molding induces algal biomatter to flow, fill gaps between adjacent wood particles, and form compatible, hydrogen-bonding-dominated interactions, densifying the wood–algae composites.[25] Algae-bound particleboards were produced by introducing 40 wt% Caulerpa, Gracilaria, Halymenia, or Ulva to wood powder and hot-pressing using the HFS conditions of each species (Fig. 5a). Binderless

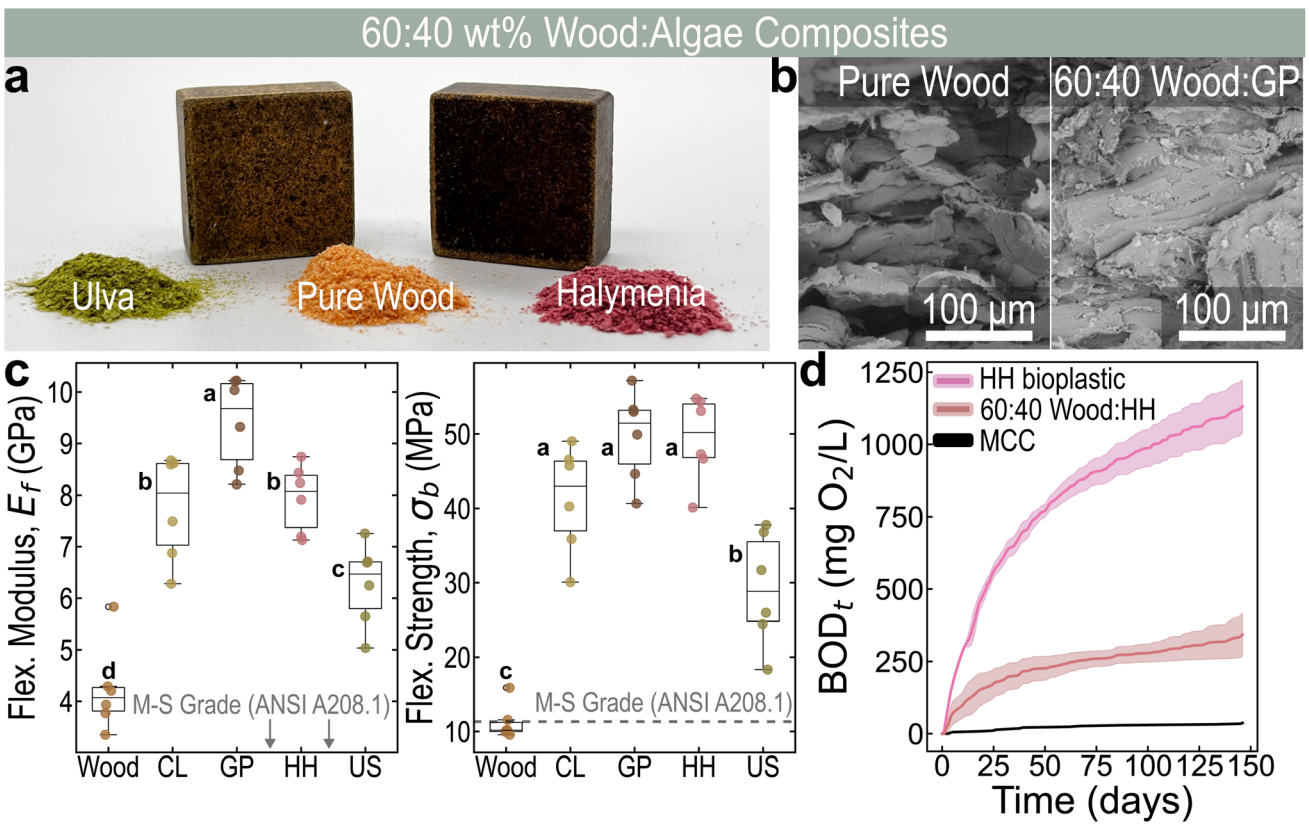

Fig. 5 (a) Photograph of 60 : 40 wood–Ulva and wood–Halymenia composites. (b) SEM images of pure wood particleboard and 60 : 40 wood–Gracilaria (GP) particleboard. (c) The flexural mechanical properties for pure wood (Wood) particleboards as well as 60 : 40 wt% wood:algae particleboard samples made using Caulerpa (CL), Gracilaria (GP), Halymenia (HH), and Ulva (US). The letters overlaid on figure (c) indicate statistically distinct groups calculated using ANOVA and Tukey HSD (significance level 0.05). The box plots overlaid on scattered data demonstrate the upper and lower quartiles while the upper and lower whiskers represent ± 1.5 of the interquartile range respectively. (d) The BOD_t (mg O_2/L of test solution) over time (days) in seawater of pure Halymenia (HH) bioplastic, 60 : 40 wt% wood–Halymenia (HH) biocomposite, and microcrystalline cellulose (MCC). The shaded region surrounding each curve shows ± 1 standard deviation of the average degradation at each point.

particleboards were also produced using pure wood powder pressed at 160 °C and 15 kN for 5 min. Comparing SEM micrographs of the wood–algae particleboards and the pure-wood particleboard (Fig. 5b and S5) confirms that algae inhabit otherwise vacant spaces in the microstructure, physically binding the material and thereby serving as an adhesive. The adhesion of the wood particles by the macroalgae produces bonded particleboards with an average density 15.6% greater than that of the pure wood control (Table S5).

The flexural properties of 60–40 wt% algae-bonded wood particleboards are shown in Fig. 5c. As for the algal bioplastics, the materials adhered using the red algae, Halymenia and Gracilaria, exhibit the greatest average flexural modulus, strength, and toughness. Unlike the pure macroalgae bioplastics, the Gracilaria-bonded material has both higher average flexural stiffness and higher average flexural strength than the Halymenia-bonded material. The performance of the Caulerpa-adhered particleboards relative to the Rhodophyta particleboards also differ slightly from the trend observed for the bioplastics; the flexural strength and stiffness of the Caulerpa particleboard are statistically similar to those of the Halymenia particleboard. In fact, comparing the algal-bonded particleboards to their corresponding bioplastics and the pure wood particleboard reveals that the relationship between their mechanical properties is non-uniform across the four macroalgae (Table S5). Combining different macroalgae and wood at the same ratio does not yield mechanical properties governed by the rule of mixtures for specimens prepared under the same processing conditions. For some species, the algal-bonded particleboards demonstrate flexural strength and stiffness greater than (Caulerpa), or approximately equal to (Gracilaria and Ulva), those of the bioplastic made using the same species, while others exhibit lower relative performance (Halymenia). The diverse relationships between the algal bioplastics and the algal-bonded particleboards of the same species may be related to variable densification and secondary bonding interactions between algae and wood. Decreasing density of the particleboards relative to the bioplastics could correspond to an increasing volume of voids within the morphology contributing to stress-concentration and crack initiation and propagation. Additionally, different ratios of sulfated to neutral polysaccharides within each species may affect the degree of intermolecular hydrogen bond formation between algae and wood in the bonded particleboards. Species with a higher density of hydoxyl groups, rather than sulfated groups, may form more stable hydrogen bonded networks with the lignocellulosic biopolymers present in the wood.[86] Together, these two factors could explain why Halymenia-bonded particleboards exhibit lower flexural strength and stiffness than the pure Halymenia bioplastics. Halymenia has a relatively high sulfate content (Fig. 1c and Table S4) and forms particleboards with a density less than that of the pure bioplastics (Table S5). And while the density of Caulerpa-bonded and Gracilaria-bonded particleboards is also lower than that of their pure algal counterparts, these two species have very low concentrations of sulfur and sulfated polysaccharides (Fig. 1c), likely explaining their favorable mechanical properties (especially for the Caulerpa-bonded particleboard). Finally Ulva, like Halymenia, has a relatively high concentration of sulfated polysaccharides (Fig. 1c); however the density of the Ulva-bonded particle boards is greater than that of the Ulva bioplastics prepared using the same hot-pressing conditions. In this case, increased density could explain why the Ulva-bonded particleboards perform similarly to the pure bioplastic.

Previously it was hypothesized that the differences in the Halymenia and Caulerpa bioplastic mechanical properties are driven by differences in the protein content and characteristics. The similarities in the particleboard performances could suggest that dynamic protein diffusion and aggregation play a lesser role in particle board formation (adhesive function) than in bioplastic cohesion (cohesive function). It could be that the extent of protein aggregation required for the densification of a network of wood particles is less than that required to achieve cohesion in pure macroalgae, and so the importance of protein in particleboards relative to other components, like polysaccharides, decreases. Additionally, the optimal pressing conditions for the algae-bonded wood particlebonds may be different from those of the pure bioplastics or the pure wood.[25] Identifying the ideal processing conditions for algal-bonded wood particleboards in future studies could affect the relationships between the maximum bioplastic and particle board mechanical properties. Potential optimization notwithstanding, each of the wood–algae composites significantly outperforms the pressed wood control material. The addition of 40 wt% algal biomatter to the particleboard feedstock improves the flexural modulus by 62.5–112.5% and the flexural strength by 180–500%. The flexural performance of the wood–algae particleboards also considerably surpasses the standard performance for M-S grade particleboards as prescribed by ANSI A208.1 (Fig. 5c).

In addition to mechanical durability, biodegradability and fire retardancy are important considerations for developing sustainable and effective construction materials. Wood:algae particleboards demonstrate respectable biodegradability in seawater (Fig. 5d) and also exhibit impressive flame retardance. Fig. 6a portrays the flame resistance of the wood–algae particleboards and the pure wood control. Here, the flame resistance is expressed as the length of time after the composites are removed from an open flame until they self-extinguish or are fully consumed. As expected, after exposure to flame, the pure wood particleboards completely burn-up. The 3 cm test specimens burn steadily for 42.3 ± 3.2 s (Fig. 6a), leaving fully charred remnants (Fig. 6b). By contrast, each of the 60–40 wt% wood–algae composites self-extinguish after approximately 5 seconds (Fig. 6a). Slight local charring is observed at the sites where combustion occurs, but the fire does not propagate after removal from the flame (Fig. 6b). While the Halymenia composites self-extinguished after the shortest time (3.0 ± 4.0 s), each of the wood–algae particleboards exhibited statistically similar extinction times ($p > 0.18$) on account of bimodal burning behavior (Fig. 6b). The wood–algae composites either sustained a small flame, which extinguished after approximately 10 seconds (self-extinction mode 1), or ceased burning immediately following removal from the ignition source (self-extinction mode 2) (Fig. 6b). The occurrence of multiple

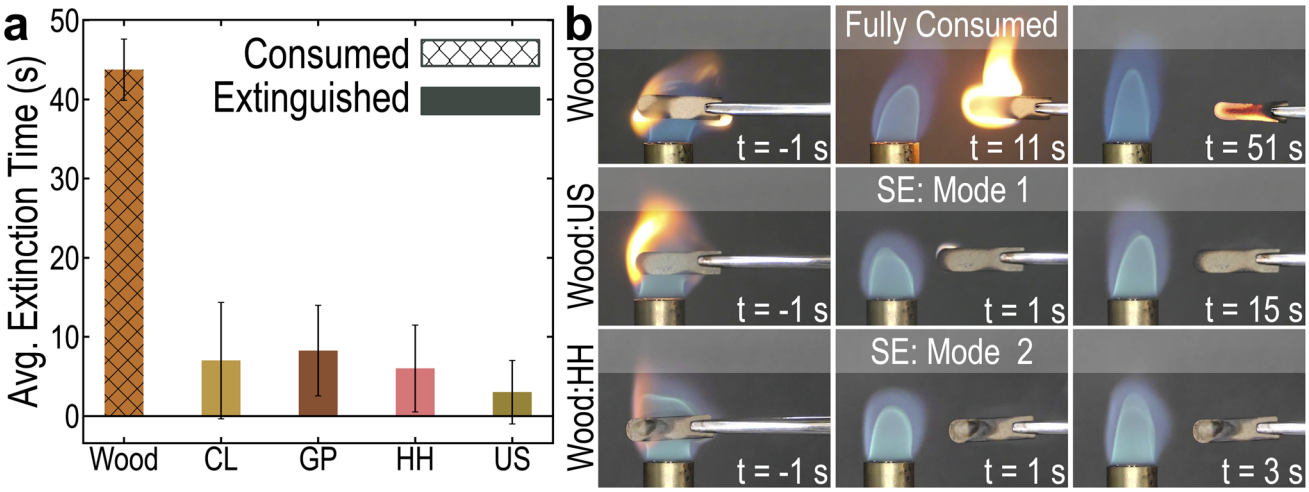

Fig. 6 (a) The time until extinction after withdrawal from flame for pure wood (Wood) particleboards as well as 60 : 40 wt% wood : algae particleboard samples made using Caulerpa (CL), Gracilaria (GP), Halymenia (HH), and Ulva (US). The error bars in (a) indicate ± 1 standard deviation. (b) Exemplar photographs of particleboard samples immediately before being withdrawn from the flame ($t = -1$ s) and during burning. Images were chosen for three samples (pure wood, 60 : 40 wood : US, and 60 : 40 wood : HH) representative of the three flame extinction modes: full consumption, delayed self-extinction (SE: Mode 1), or instantaneous self-extinction (SE: Mode 2).

burning modes explains the large variance in the extinction time of the wood–algae particleboards.

The self-extinction and inherent fire retardancy induced by the algal adhesives may be attributed to favorable aspects of their chemical compositions. Elemental analysis of the algal species indicated that each has significant concentrations of nitrogen (largely from proteins), chlorine, potassium, and sodium (likely from salt residue), and traces of silicon and phosphorus (Table S4). The salts and other inorganic residues present in the seaweed at relatively high concentrations (Table 1) are noncombustible and may therefore imbue flame retardant properties by decreasing the total concentration of flammable material. Additionally, several nitrogen and phosphorous containing compounds have been observed to decrease flame propagation during combustion.[87] Nitrogenous and phosphoric organic molecules may form insulating char layers or inert gases at high temperatures that starve flames of fuel or insulate combustible material.[87] Some proteins may even enhance the ability of biopolymers like cellulose to form insulative char layers.[88] Overall, the flame resistance and impressive mechanical performance of wood–algae fiber boards qualify the Hawaiian algae as potential replacements, or even improvements, for synthetic particleboard adhesives.

3.5 Sustainability assessment of macroalgal bioplastics and algal-bonded wood particleboards

The sustainability of the macroalgal bioplastics and algal-bonded wood particleboards is evaluated by considering the environmental effects of their fabrication and end-of-life fate. Typically, cradle-to-gate life cycle analysis (LCA) is performed to calculate the effects of material production on several environmental impact categories such as climate change, acidification, eutrophication, and ozone depletion. While a comprehensive LCA was not performed for each of the eight novel materials developed herein, our recent study did, in fact, implement a harmonized cradle-to-gate LCA to compare the production of macroalgal plastics made using *Saccharina latissima* (sugar kelp) to polylactic acid (PLA), one of the most commercially dominant bioplastics today.[89] By comparing the production of both materials at the lab scale, it was determined that the macroalgal bioplastics exhibited on average 47% less environmental harm than PLA over a broad range of impact categories. Notably, the fabrication of sugar kelp bioplastics resulted in a 63% lower contribution to climate change than PLA for the same functional unit and production scale. Because near identical methods were utilized to prepare and manufacture both the Hawaiian macroalgae and sugar kelp, the bioplastics produced with Caulerpa, Gracilaria, Halymenia, and Ulva likely have very similar environmental impacts to those produced using sugar kelp.[89] LCA of a similar scope and depth has not been performed for algal-adhered wood particleboards; however, initial estimates have been made for the carbon dioxide sequestration of such materials.[25] It was estimated that wood particleboards bound with 40 wt% Ulva could sequester 1.21 kg CO_2 per kg particleboard for tens of years. This carbon sequestration could contribute to a diminished climate change impact.[90]

To evaluate the end of life impact of algal bioplastics and algal-bonded wood particleboards, the degradation of Halymenia plastic and 60 : 40 wood : Halymenia particleboard in seawater was measured for approximately 150 days. Measuring biodegradability approximates the environmental persistence of materials that escape waste collection and enter the natural environment. Biodegradability can be measured using soil burial tests but respirometry was performed here to directly quantify oxygen consumption during degradation and to avoid errors associated with specimen handling and moisture control. Because of limited time and equipment, the

biodegradability was only evaluated for these two materials. However, we believe that the trends observed for the Halymenia bioplastics and wood particleboards are likely representative of the materials made with other species. The biochemical oxygen consumption during biodegradation in sea water of wood:-Halymenia particleboard, pure HFS Halymenia bioplastic, and the microcrystalline cellulose (MCC) control is shown in Fig. 5d. Over time, the algal biomaterials degrade and their constituents react with oxygen to form byproducts including CO_2. Both the bioplastic and particleboard are consuming oxygen over time, indicating significant biodegradation. Notably, the Halymenia bioplastic specimens consume more than four times the oxygen than the wood:Halymenia particleboards over the same length of time, potentially because of the specific enzymes employed by the microbial populations present in the sea water used. The extremely low consumption of oxygen by the MCC control indicates that the waterborne microbes do not employ cellulase, thus preventing the biodegradation of the woody fraction of the wood:Halymenia composites.[91] Furthermore, the 40 wt% of Halymenia in the wood composites is not consuming oxygen at the same rate as the bioplastic. Assuming that the Douglas fir is not degrading during the time period observed, the composite sample consumed only 28.7% of the oxygen consumed by the bioplastic, as opposed to the expected 40%. The discrepancy suggests that the woody fraction of the biocomposite may be inhibiting microbial access to the algal fraction and delaying biodegradation.

While the BOD_t is a strictly quantitative, albeit indirect, measure of degradation, the approximate biodegradability of algal biomaterials can also be calculated by combining the BOD_t with best efforts to calculate biomatter ThOD and by using eqn (1) (Tables S1 and S2). Using this technique, the biodegradation percentages over time for HFS Halymenia bioplastics, 60 : 40 wood : Halymenia biocomposites, and MCC were calculated and are presented in Fig. S6. After 147 days, it was calculated that the Halymenia bioplastics and wood composites are 102.5 ± 8.6% and 25.8 ± 6.3% degraded, respectively. The calculated value of bioplastic biodegradation (D_t) in excess of 100% likely stems from excess oxygen consumption in the reaction vessels, potentially related to microbial proliferation. However, despite subtleties related to the microbiome, the bioplastics and composite particleboards degrade significantly over the time period studied and could limit environmental accumulation associated with plastics and wood construction materials.

4 Conclusions

This study demonstrates that native Hawaiian macroalgae can serve as local, sustainable, and effective feedstocks for the direct production of structurally load-bearing bioproducts, including self-bonded bioplastics and algae-bonded particleboards. Central to this approach is the deliberate use of whole, unfractionated macroalgal biomatter, which preserves native chemical complexity while reducing processing steps, energy input, and reliance on chemical extraction. The successful fabrication of two structurally distinct material classes from the same untreated biomatter highlights the versatility of macroalgal biomatter as a feedstock for scalable materials processing. A key contribution of this work is the comprehensive, species-resolved characterization of macroalgal composition, encompassing carbohydrate speciation, protein molecular weight determination, and the measurement of the lipid and inorganic fractions. By pairing this compositional analysis with systematic materials testing and biomolecular characterization, correlations between native biomatter chemistry, powder morphology, and mechanical performance were identified. Evaluation of the micromorphology of all macroalgal bioplastics revealed a combination of self-bonded matrices and areas of intact or compacted tissues, indicating that both chemical interactions and physical consolidation contribute to load-bearing behavior. Mechanical trends further suggest that both protein concentration and protein molecular weight influence self-bonding efficiency. Species containing lower molecular weight proteins, such as Gracilaria, exhibited higher stiffness and strength than species with broader or higher molecular weight protein distributions, such as Ulva, at comparable protein contents, consistent with enhanced molecular mobility and intermolecular interactions. In regard to the algae-bonded particleboards, SEM confirmed that the macroalgal powders filled spaces between wood particles, acting as an adhesive and improving the mechanical performance of the particleboards. Impressive self-extinguishing properties of the wood–algae particleboards were also observed, likely due to the inorganic residues and flame-resistant elements present in the macroalgal biomatter. Future studies can build on this foundation to further resolve component-level structure–property relationships and expand scalable processing routes for macroalgal biomatter across a broader range of material applications. Overall, this work establishes a framework for utilizing deep compositional analysis as a tool to evaluate the suitability of different macroalgae species as feedstocks for direct, non-extractive processing into high-performance materials.

Author contributions

Ian R. Campbell: data curation, formal analysis, investigation, visualization, writing – original draft, writing – review & editing. Ty Shitanaka: data Curation, formal analysis, investigation, visualization, writing – original draft, writing – review & editing. Hannah Egan: investigation. Manpreet Kaur: investigation. Samir Kumar Khanal: conceptualization, supervision, writing – review & editing. Eleftheria Roumeli: conceptualization, supervision, writing – review & editing. All authors have given approval to the final version of the manuscript.

Conflicts of interest

There are no conflicts to declare.

Data availability

The data supporting this article have been included as part of the supplementary information (SI). Supplementary

information: Tables S1–S5 and Fig. S1–S6. See DOI: https://doi.org/10.1039/d6su00024j.

Acknowledgements

The authors would like to gratefully acknowledge Todd Low and the Hawai'i Department of Agriculture and Biosecurity for the financial support provided through a grant (contract no. 70811). This work was also funded in part by the National Science Foundation (NSF) DMREF Award #2323976. This work was supported by GlycoMIP, a National Science Foundation Materials Innovation Platform funded through Cooperative Agreement DMR-1933525. I. R. C. acknowledges funding from the NSF Graduate Research Fellowship under Grant No. DGE-2140004. The authors thank the Ānuenue Fisheries Research Center and Ocean Era, LLC. for donating macroalgae for this project, as well as Dr Zhi-Yan (Rock) and Danielle Hull for assistance with the lipid and fatty acid, and CHN analyses, respectively. We also want to thank Dr Paul Grandgeorge and Dr Surendra K. C. for useful discussions during the early stages of this work.

Notes and references

1 C. M. Duarte, A. Bruhn and D. Krause-Jensen, *Nat Sustainability*, 2021, **5**, 185–193.
2 L. Zhang, W. Liao, Y. Huang, Y. Wen, Y. Chu and C. Zhao, *Food Prod., Process. Nutr.*, 2022, **4**, 23.
3 L. Janke, *J. Ind. Ecol.*, 2024, **28**, 1256–1269.
4 S. García-Poza, D. Pacheco, J. Cotas, J. C. Marques, L. Pereira and A. M. M. Gonçalves, *Integr. Environ. Assess. Manage.*, 2022, **18**, 1148–1161.
5 K. Larsen-Ledet, T. Boderskov, B. Olesen, M. M. Larsen, N. Simonsen, E. R. Christiansen, L. H. Nielsen, L.-A. T. Tran, S. D'Hondt, O. De Clerck and A. Bruhn, *Algal Res.*, 2025, **85**, 103858.
6 D. Krause-Jensen and C. M. Duarte, *Nat. Geosci.*, 2016, **9**, 737–742.
7 C. M. Duarte, J. Wu, X. Xiao, A. Bruhn and D. Krause-Jensen, *Front. Mar. Sci.*, 2017, **4**, 100.
8 M. Eggertsen, J. T. Fumo, L. M. Rasmusson, U. Bergström, C. M. Smith and A. R. Sherwood, *Biol. Invasions.*, 2025, **27**, 148.
9 B.-T. Dang, X.-T. Bui, D. P. H. Tran, H. Hao Ngo, L. D. Nghiem, T.-K.-D. Hoang, P.-T. Nguyen, H. H. Nguyen, T.-K.-Q. Vo, C. Lin, K. Yi Andrew Lin and S. Varjani, *Bioresour. Technol.*, 2022, **347**, 126698.
10 Q. Li, M. Jalalah, S. A. Alsareii, F. A. Harraz, A. A. Almadiy, Y. Yang and E.-S. Salama, *Environ. Dev. Sustain.*, 2025, **27**, 8383–8401.
11 S. Kammler, A. Malvis Romero, C. Burkhardt, L. Baruth, G. Antranikian, A. Liese and M. Kaltschmitt, *Biomass Bioenergy*, 2024, **183**, 107105.
12 M. Narayanan, *Algal Res.*, 2024, **82**, 103687.
13 J. M. Santos, B. C. Jesus, H. Ribeiro, A. Martins, J. Marto, M. Fitas, P. Pinto, C. Alves, J. Silva, R. Pedrosa and I. M. Marrucho, *Algal Res.*, 2024, **79**, 103438.
14 C. Zhang, P.-L. Show and S.-H. Ho, *Bioresour. Technol.*, 2019, **289**, 121700.
15 M. Escura, A.-M. Koussoroplis and C. Desvilettes, *Limnol. Oceanogr.*, 2025, **70**, 1059–1074.
16 Y. Zheng, Y. Li, Y. Yang, Y. Zhang, D. Wang, P. Wang, A. C. Y. Wong, Y. S. Y. Hsieh and D. Wang, *J. Agric. Food Chem.*, 2022, **70**, 1438–1453.
17 A. B. García, E. Longo, M. C. Murillo and R. Bermejo, *Molecules*, 2021, **26**, 297.
18 K. Scardifield, N. McLean, U. Kuzhiumparambil, P. J. Ralph, N. Neveux, G. Isaac and T. Schork, *J. Appl. Phycol.*, 2024, **36**, 935–950.
19 A. K. Mondal, C. Hinkley, L. Krishnan, N. Ravi, F. Akter, P. Ralph and U. Kuzhiumparambil, *RSC Sustainability*, 2024, **2**, 1828–1836.
20 M.-Y. Lin, P. Grandgeorge, A. M. Jimenez, B. H. Nguyen and E. Roumeli, *ACS Sustain. Chem. Eng.*, 2023, **11**, 8242–8254.
21 B. Lou, M. Parker and E. Roumeli, *BioResources*, 2025, **20**, 4152–4173.
22 M. A. Zeller, R. Hunt, A. Jones and S. Sharma, *J. Appl. Polym. Sci.*, 2013, **130**, 3263–3275.
23 C. Mathiot, P. Ponge, B. Gallard, J.-F. Sassi, F. Delrue and N. Le Moigne, *Carbohydr. Polym.*, 2019, **208**, 142–151.
24 H. Iyer, P. Grandgeorge, A. M. Jimenez, I. R. Campbell, M. Parker, M. Holden, M. Venkatesh, M. Nelsen, B. Nguyen and E. Roumeli, *Adv. Funct. Mater.*, 2023, **33**, 2302067.
25 P. Grandgeorge, I. R. Campbell, H. Nguyen, R. Brain, M. Parker, S. Edmundson, D. Rose, K. Homolke, C. Subban and E. Roumeli, *MRS Bull.*, 2024, **49**, 787–801.
26 P. Stegmann, V. Daioglou, M. Londo, D. P. van Vuuren and M. Junginger, *Nature*, 2022, **612**, 272–276.
27 R. Geyer, J. R. Jambeck and K. L. Law, *Sci. Adv.*, 2017, **3**, e1700782.
28 A. J. Nihart, M. A. Garcia, E. El Hayek, R. Liu, M. Olewine, J. D. Kingston, E. F. Castillo, R. R. Gullapalli, T. Howard, B. Bleske, J. Scott, J. Gonzalez-Estrella, J. M. Gross, M. Spilde, N. L. Adolphi, D. F. Gallego, H. S. Jarrell, G. Dvorscak, M. E. Zuluaga-Ruiz, A. B. West and M. J. Campen, *Nat. Med.*, 2025, **31**, 1114–1119.
29 I. R. Campbell, Z. Dong, P. Grandgeorge, A. M. Jimenez, E. R. Rhodes, E. Lee, S. Edmundson, C. V. Subban, K. G. Sprenger and E. Roumeli, *Matter*, 2025, 101941.
30 B. A. Yoza and E. M. Masutani, *Environ. Technol.*, 2013, **34**, 1859–1867.
31 W. APHA, AWWA, *Standard Methods for the Examination of Water and Wastewater*, American Public Health Association, American Water Works Association, Water Environment Federation, 23rd edn, 2017, ch. 2540 Solids.
32 S. V. Wychen and L. M. L. Laurens, *Golden, Colorado*, National Renewable Energy Laboratory, 2023.
33 W. Chen, L. Gao, L. Song, M. Sommerfeld and Q. Hu, *Algal Res.*, 2023, **70**, 102986.
34 S. P. Slocombe, M. Ross, N. Thomas, S. McNeill and M. S. Stanley, *Bioresour. Technol.*, 2013, **129**, 51–57.
35 Z. Wang and C. Benning, *J. Visualized Exp.*, 2011, 2518.

36 P. B. Torres, A. Nagai, C. E. P. Jara, J. P. Santos, F. Chow and D. Y. A. C. dos Santos, *Ocean and Coastal Research*, 2021, **69**, e21021.
37 S. Ahmad, A. Singh, W. Akram, A. Upadhyay and G. S. Abrol, *J. Food Sci.*, 2025, **90**, e17618.
38 K. L. Van Alstyne and M. P. Puglisi, *Aquat. Sci.*, 2007, **69**, 394–402.
39 S. V. Wychen and L. M. L. Laurens, *Determination of Total Carbohydrates in Algal Biomass: Laboratory Analytical Procedure (LAP)*, National renewable energy laboratory technical report, 2023.
40 L. Niu, H. Zhang, Z. Wu, Y. Wang, H. Liu, X. Wu and W. Wang, *PLoS ONE*, 2018, **13**, e0202238.
41 W. Stoffel, F. Chu and E. H. Ahrens, *Anal. Chem.*, 1959, **31**, 307–308.
42 *ASTM6691, Standard Test Method for Determining Aerobic Biodegradation of Plastic Materials in the Marine Environment by a Defined Microbial Consortium or Natural Sea Water Inoculum*, American society for testing and materials standard, 2018.
43 *ISO14851, Determination of the Ultimate Aerobic Biodegradability of Plastic Materials in an Aqueous Medium — Method by Measuring the Oxygen Demand in a Closed Respirometer*, International organization for standardization standard, 2019.
44 A. W. Pupulawaththa, MSc thesis, Universitetet i Sørøst-Norge, 2018.
45 J. Schindelin, I. Arganda-Carreras, E. Frise, V. Kaynig, M. Longair, T. Pietzsch, S. Preibisch, C. Rueden, S. Saalfeld, B. Schmid, J.-Y. Tinevez, D. J. White, V. Hartenstein, K. Eliceiri, P. Tomancak and A. Cardona, *Nat. Methods*, 2012, **9**, 676–682.
46 Z. Shao and D. Duan, *Front. Plant Sci.*, 2022, **13**, 90283.
47 É. Chassé, M. V. Curtasu, M. Battelli, K. E. Bach Knudsen, A. Bruhn and M. O. Nielsen, *Algal Res.*, 2025, **85**, 103878.
48 M. Kaur, T. Shitanaka, K. Surendra and S. K. Khanal, *Crit. Rev. Food Sci. Nutr.*, 2024, 1–23.
49 J. Xu, W. Liao, Y. Liu, Y. Guo, S. Jiang and C. Zhao, *Food Prod., Process. Nutr.*, 2023, **5**, 18.
50 A. Yücetepe, C. Kırkın, Z. Mertdinç, E. N. Ayar, C. Soylukan, E. Dikici, B. Özçelik and E. Ş. Okudan, *Food Prod., Process. Nutr.*, 2024, **6**, 84.
51 J. Muthukumar, R. Chidambaram and S. Sukumaran, *J. Food Sci. Technol.*, 2021, **58**, 2453–2466.
52 Y. Sun, G. Gong, Y. Guo, Z. Wang, S. Song, B. Zhu, L. Zhao and J. Jiang, *Int. J. Biol. Macromol.*, 2018, **108**, 314–323.
53 T. Konishi, I. Nakata, Y. Miyagi and M. Tako, *J. Appl. Glycosci.*, 2012, **59**, 161–163.
54 M. Lahaye and A. Robic, *Biomacromolecules*, 2007, **8**, 1765–1774.
55 N. Wahlström, U. Edlund, H. Pavia, G. Toth, A. Jaworski, A. J. Pell, F. X. Choong, H. Shirani, K. P. R. Nilsson and A. Richter-Dahlfors, *Cellulose*, 2020, **27**, 3707–3725.
56 A. I. Usov, *Food Hydrocolloids*, 1998, **12**, 301–308.
57 F. C. N. Barros, D. C. da Silva, V. G. Sombra, J. S. Maciel, J. P. A. Feitosa, A. L. P. Freitas and R. C. M. de Paula, *Carbohydr. Polym.*, 2013, **92**, 598–603.
58 A. T. Mulio, C.-S. Chiu, Y.-J. Chan, W.-C. Lu and P.-H. Li, *Food Front.*, 2025, **6**, 2129–2143.
59 T. A. Fenoradosoa, C. Delattre, C. Laroche, A. Wadouachi, V. Dulong, L. Picton, P. Andriamadio and P. Michaud, *Int. J. Biol. Macromol.*, 2009, **45**, 140–145.
60 S. Yu, A. Blennow, M. Bojko, F. Madsen, C. E. Olsen and S. B. Engelsen, *Starch - Stärke*, 2002, **54**, 66–74.
61 S. Augyte, N. A. Sims, K. Martin, S. Van Wychen, B. Panczak, H. Alt, R. Nelson and L. M. L. Laurens, *Plants*, 2023, **12**, 3524.
62 J. Samarathunga, I. Wijesekara, M. Jayasinghe, G. Mahajan and V. G. Warke, *J. Food Meas. Charact.*, 2025, **19**, 38–48.
63 S. Caronni, F. Addis, M. A. Delaria, R. Gentili, C. Montagnani, A. Navone, P. Panzalis and S. Citterio, *J. Appl. Phycol.*, 2021, **33**, 2485–2496.
64 H. P. T. Nguyen, M. Morançais, P. Déléris, J. Fleurence, C. T. Nguyen-Le, K. H. Vo and J. Dumay, *J. Appl. Phycol.*, 2020, **32**, 553–561.
65 S. Malairaj, S. Muthu, V. B. Gopal, P. Perumal and R. Ramasamy, *J. Chromatogr. A*, 2016, **1454**, 120–126.
66 H. Pereira, L. Barreira, F. Figueiredo, L. Custódio, C. Vizetto-Duarte, C. Polo, E. Rešek, A. Engelen and J. Varela, *Mar. Drugs*, 2012, **10**, 1920–1935.
67 I. A. Guschina and J. L. Harwood, *Prog. Lipid Res.*, 2006, **45**, 160–186.
68 N. Gnayem, R. Unis, R. Gnaim, A. Chemodanov, A. Israel, J. Gnaim and A. Golberg, *Life*, 2025, **15**, 57.
69 D. Britton, M. Schmid, A. T. Revill, P. Virtue, P. D. Nichols, C. L. Hurd and C. N. Mundy, *J. Appl. Phycol.*, 2021, **33**, 603–616.
70 J. M. Greene, J. Gulden, G. Wood, M. Huesemann and J. C. Quinn, *Algal Res.*, 2020, **51**, 102032.
71 R. Chandra, H. M. N. Iqbal, G. Vishal, H.-S. Lee and S. Nagra, *Bioresour. Technol.*, 2019, **278**, 346–359.
72 M. Z. Khan, S. K. Srivastava and M. Gupta, *J. Reinf. Plast. Compos.*, 2018, **37**, 1435–1455.
73 S. Tesfaw, T. M. Bogale and O. Fatoba, *Mater. Today: Proc.*, 2022, **62**, 3103–3113.
74 J.-Z. Liang, S.-Y. Zou and Q. Du, *Polym. Test.*, 2018, **70**, 434–440.
75 H. Y. Sohn and C. Moreland, *Can. J. Chem. Eng.*, 1968, **46**, 162–167.
76 T. Li, H. Sun, B. Wu, H. Han, D. Li, J.-K. Wang, J. Zhang, J. Huang and D. Sun, *Mater. Des.*, 2020, **195**, 109003.
77 M. G. A. Vieira, M. A. da Silva, L. O. dos Santos and M. M. Beppu, *Eur. Polym. J.*, 2011, **47**, 254–263.
78 E. D'Agnolo, R. Rizzo, S. Paoletti and E. Murano, *Phytochemistry*, 1994, **35**, 693–696.
79 R. Rajan, S. Ahmed, N. Sharma, N. Kumar, A. Debas and K. Matsumura, *Mater. Adv.*, 2021, **2**, 1139–1176.
80 J.-W. Rhim, *J. Food Sci.*, 2012, **77**, N66–N73.
81 J.-W. Rhim and L.-F. Wang, *Carbohydr. Polym.*, 2013, **96**, 71–81.
82 N. Rhein-Knudsen, M. T. Ale, F. Ajalloueian, L. Yu and A. S. Meyer, *Food Hydrocolloids*, 2017, **63**, 50–58.
83 A. Fuchs, E. Hupfeld and V. Sieber, *Carbohydr. Polym.*, 2024, **333**, 121930.

84 J. L. Fredricks, A. M. Jimenez, P. Grandgeorge, R. Meidl, E. Law, J. Fan and E. Roumeli, *J. Polym. Sci.*, 2023, **61**, 2585–2632.
85 O. C. Ulker and O. Ulker, *BioResources*, 2019, **14**, 7465–7493.
86 K. Bu, Y. Wang, L. Qiao, L. Xing, C. Du and P. Wang, *Food Hydrocolloids*, 2026, **172**, 111900.
87 H. Vahabi, F. Laoutid, M. Mehrpouya, M. R. Saeb and P. Dubois, *Mater. Sci. Eng., R*, 2021, **144**, 100604.
88 F. Carosio, A. Di Blasio, F. Cuttica, J. Alongi and G. Malucelli, *Ind. Eng. Chem. Res.*, 2014, **53**, 3917–3923.
89 M.-Y. Lin, R. D. Colwell, I. R. Campbell, K. Liao and E. Roumeli, *ACS Sustain. Chem. Eng.*, 2026, **14**, 2010–2029.
90 S. Cordier, P. Blanchet, F. Robichaud and B. Amor, 2022, **226**, 109695.
91 R. Nagamine, K. Kobayashi, R. Kusumi and M. Wada, *Cellulose*, 2022, **29**, 2917–2926.